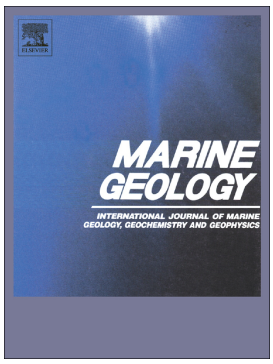

A new approach to assess ancient marine slope instability using a bivariate statistical method

Aldina Piedade, Tiago M. Alves, José Luís Zêzere

PII: S0025-3227(17)30414-0
DOI: doi:10.1016/j.margeo.2018.04.006
Reference: MARGO 5783

To appear in: *Marine Geology*

Received date: 31 August 2017
Revised date: 26 March 2018
Accepted date: 15 April 2018

Please cite this article as: Aldina Piedade, Tiago M. Alves, José Luís Zêzere , A new approach to assess ancient marine slope instability using a bivariate statistical method. The address for the corresponding author was captured as affiliation for all authors. Please check if appropriate. Margo(2017), doi:10.1016/j.margeo.2018.04.006

A new approach to assess ancient marine slope instability using a bivariate statistical method

Aldina Piedade[1,2], Tiago. M. Alves[1] José Luís Zêzere,[2]

[1]3D Seismic Lab. School of Earth and Ocean Sciences, Cardiff University, Main Building, Park Place, Cardiff, CF10 3AT, The United Kingdom

[2] RISKam, Centro de Estudos Geográficos, IGOT, Universidade de Lisboa, Portugal

E-mail address: aldinapiedade@campus.ul.pt

Abstract

Slope instability is one of the most effective processes shaping the seafloor of continental margins. The end-product of slope instability, mass-transport deposits (MTDs), have been documented in the literature using diverse approaches. This paper tests a new methodology, applied to a region offshore Espírito Santo (SE Brazil), for the evaluation of MTDs' occurrence on continental slopes. An MTD inventory was, in a first stage, made for a cropped region of SE Brazil using a high resolution three-dimensional (3D) seismic volume. This MTD inventory consists of four MTDs that were mapped and exported into a Geographic Information Systems (GIS) database. MTD favourability scores were then computed in a second stage using algorithms based on statistical/probabilistic analyses (Information Value Method), over unique terrain conditions, in a raster basis. Terrain attributes derived from the Digital Terrain Model (DTM) were used as proxies to several driving factors of MTDs, and as predictors in the models. As a result, three models are discussed independently in this paper, according to the different datasets used to interpret MTDs (Models 1, 2 and 3). The results were prepared by sorting all pixels according their favourability value, in descending order, with robustness and accuracy of the MTD favourability models having been evaluated by success-rate curves. The curves aided in the quantitative interpretation of the models expressing their goodness of fit to the interpreted MTDs. This work is important because the outputs resulting from the methodology confirm that this new method can be applied to submarine slopes. From the three models, Model 3 obtained the highest goodness of fit (0.862). Based on our results, a sensitivity analysis was undertaken and key predisposing factors were identified. The new

methodology in this work has the potential to become a very important and valid approach for the recognition of submarine slopes prone to failure on continental margins around the world.

Keywords: Bivariate Informative Value Method, modelling, mass-transport deposits, offshore slope instability, statistic predictive models, Offshore Espírito Santo Basin (SE Brazil).

1. Introduction

Submarine slope instability is one of the main natural hazards affecting continental margins, and can result in direct and indirect damage to seafloor infrastructure (Dai et al., 2002). Submarine slope instability occurs when there is a significant reduction in the shear strength of continental slope sediments, usually at the location of a future basal glide plane, or shear zone (Varnes, 1978, Hampton et al., 1996, Alves and Lourenço, 2010, Alves, 2015). The last few decades witnessed significant improvements in submarine landslide characterisation, and in the understanding of the local conditions leading to slope instability at small and large scales of observation (Nadim, 2006, Hough et al., 2011, Gilbert et al., 2013, Rodríguez-Ochoa et al., 2015). The development of new techniques such as 3D seismic interpretation has greatly contributed towards the understanding of submarine slope instability, and allowed the integration of geophysical and 3D-imagery in spatial analysis tools such as Geographic Information Systems (GIS). In fact the use of GIS techniques, thus far applied to onshore risk assessments, in the characterisation of offshore instability processes has improved our knowledge of the factors that trigger such catastrophic events (McAdoo, 2000). By combining 3D seismic datasets with GIS databases, one can explore the different tools used in GIS spatial analyses (Haneberg et al., 2015), taking advantage of methodologies widely tested onshore.

Offshore slope stability analyses have recently benefited from improvements in data acquisition, data processing and analytical techniques. Some of these improvements allow the computation of models representing the spatial distribution of the physical parameters that may influence the occurrence of mass movements (Urgeles et al., 2006, Micallef et al., 2007, Micallef, 2011, Li et al., 2014, Haneberg et al., 2015). Hence, susceptibility analyses are undertaken with the final aim of understanding the conditions and

parameters that favour the occurrence of mass movements in specific locations (Soeters and Van Westen, 1996, van Westen et al., 2006, Thiery et al., 2007, van Westen et al., 2008). In their final stages, susceptibility analyses can identify regions where, under a set of favourable conditions, mass movements will likely occur. A great part of slope instability predictive studies uses statistical methods that cross-correlate predisposing factors with inventories of (past) events, within a GIS environment (van Westen et al., 1997, Carrara et al., 1999, Piedade et al., 2010, Pereira et al., 2012, Borrell et al., 2016). Slope stability analyses are usually based on a deterministic approach, where the level of safety of a slope is quantified by a 'safety factor' (Nadim, 2006). The factors that cause slope failure include predisposing, preparatory and triggering factors (Glade and Crozier, 2005).

In this paper we use topography information from a palaeo-slope to build up a set of possible predisposing factors (e.g. Glade and Crozier, 2005, Pereira et al., 2012) that were present during slope failure in parts of the offshore Espírito Santo Basin, SE Brazil (Fig. 1). This was undertaken via integration of data from the interpreted 3D seismic volume into GIS using a statistical method, the Informative Value (IV) (Yin and Yan, 1988). As a result of our approach we aim at: (a) determining a set of predisposing factors that can reflect the natural conditions (exclusive from the topographic proxies) for the occurrence of mass-transport deposits (MTDs) on continental slopes; (b) performing a bivariate statistical model that integrates the mapped MTDs and the predisposing factors into GIS, with the ultimate step of compiling a predictive map of MTDs' occurrence; (c) determining the favourability scores of predisposing factors that induce the occurrence of MTDs; (d) validating the statistical model applied using success-rate curves and by calculating the corresponding Area Under the Curve (AUC), and; (e) running a sensitivity analysis of the variables used for modelling in order to understand which variables influence the model in greater degree.

In summary, this paper presents a new methodology to understand how the bivariate statistical model of Informative Value (IV) responds to marine mass movements using data derived from 3D seismic volumes. If results are considered positive, marine datasets can be used to improve the methodology and largely contribute for future submarine slope assessment and the understanding of palaeo-slope failure.

2. Regional setting of the Espiríto Santo Basin

The Espírito Santo Basin is located along the SE continental margin of Brazil (Fig. 1). The basin is characterised by significant halokinesis, a result of a thick evaporite succession that having been accumulated in the region from Late Aptian to Early Albian (Fig. 2).

Halokinetic movements played an important part in the Espírito Santo Basin's evolution. Consequently, the very thick Tertiary sequence of the Espírito Santo continental slope is composed of a mixture of carbonate and clastic sediment (França et al., 2007). In such a context, mass-wasting events offshore Espírito Santo are a result of regional tectonic movements (Mohriak et al., 2008) combined with local instability phenomena related to halokinesis (Fiduk et al., 2004).

The stratigraphic interval interpreted in great detail for this study, as characterised by França et al. (2007), corresponds to the N20-N60 sequence. In the studied continental slope, this sequence comprises strata of the Rio Doce, Caravelas and Urucutuca units which are, in places, eroded by submarine channels (Fig. 2). The three stratigraphic units comprise sandstones (Rio Doce Formation), calcarenites (Caravelas member), plus turbidite sands and marls (Urucutuca Formation). As the study area is located at the mid part of the continental slope, we expect sediments with a relatively high percentage of sand. In fact, MTDs and channel-fill deposits are abundant throughout the basin after the Early Miocene. Seismic reflections in the N20-N60 sequence are chaotic to continuous, and have described in detail in the literature (e.g. França et al., 2007).

3. Methods and data

3.1 MTDs inventory, data resolution and modelling strategy

The interpreted seismic volume was acquired with a dominant frequency of 40 Hz, corresponding to vertical resolutions of ~15.6 and 19.35 m considering velocities of 3100 m/s and 2100 m/s for the deeper and shallower horizons, respectively. The frequency of the highest amplitude corresponds to the dominant frequency, which is obtained from the processing algorithm. For migrated data, horizontal resolution is equal to the bin size and is ~12.5 m for the interpreted volume (Barker et al., 1993, Fiduk et al., 2004). Bin-size and vertical resolution(s) were crucial for our depth-converted calculations.

For the purposes of this study, a seismic horizon at the base of multiple MTDs was mapped and later used as a proxy of the original topography (Fig. 3a, 3b). The horizon mapped corresponds to a high-amplitude seismic reflection (negative, in this case) at the boundary between the lower and upper Miocene strata (17-18 Ma), and covers an area of approximately 756 km^2. This topographic surface is also where the identified MTDs are placed (Fig. 3c). In this sense, the topographic surface is used in this work as a proxy Digital Terrain Model (DTM) representing the topography of a palaeo-slope over which the instability events occurred. Despite the fact that movements occurred just above this topographic surface, by our mapping process we assumed in our work that the surface was not significant affected by the downslope movement of the MTDs.

Based on this mapped topographic surface, we computed seven (7) predisposing factors that were chosen based on: a) the dataset available, b) the relative applicability of GIS tools in the submarine environment (e.g. Micallef et al., 2007, Micallef, 2011, Lecours et al., 2016). We chose these predisposing factors to identify the natural conditions related to the topography at the time of slope failure, presumed to have occurred at the end of the Miocene. We must stress, at this point, that the seven predisposing factors are originated from a 3D high-amplitude seismic reflection used to compute a proxy of topography, excluding geologic layers and faults. The rationale of this paper consists of understanding how DEM-related factors – known to be predisposing of slope instability onshore - can be applied to submarine environments and specially, palaeo-slopes, and how valid is the approach taken in this work. We recognise the importance of incorporating geological information in slope instability analyses (e.g. Borrell et al., 2016) but, considering the lack of borehole information in the study area, we considered appropriate to propose the DEM-related methodology developed in this work.

In a final stage in our analysis, three different models were compiled using: i) model 1 (M1), which considers the total area of MTDs, ii) model 2 (M2), with 1/3 of the MTDs total length, and iii) model 3 (M3), with half of the MTDs' length used in model 2. An attempt at constraining the probable rupture zone of the interpreted MTDs was undertaken by model 2 and model 3, whereas model 1 was compiled using the entire MTD area. Favourability scores were then calculated for each class of each predisposing factor (designed as independent variables) and for the three models. The models were validated through success-rate curves and corresponding AUCs.

In order to check the validity of the correlation between independent variables used in the models, we computed multicollinearity (e. g. Van Den Eeckhaut et al., 2006, Bai et al., 2010, Melo & Zêzere, 2017), through Tolerance (TOL) and variance inflation factors (VIF). In detail, values of TOL < 0.2 and VIF >2 are indicator of multicollinearity.

3.2 Predisposing factors

We chose seven predisposing factors associated with the topography present at the time of the slope failure. The predisposing factors considered were elevation, slope gradient, profile curvature, planform curvature, flow direction, flow accumulation and slope over area ratio, which are considered in the models as independent variables. All the independent variables were computed within *ArcGis Software*. Binning was fixed for five of these factors - profile curvature, planform curvature, flow direction, flow accumulation and slope area over ratio - while elevation and slope degree were chosen by adapting the binning to the topographic characteristics of the palaeo-slope.

The elevation range between the lowest and highest point of the topographic surface, after converting TWT depth into depth in metres, is considered 0 m at the lowest part of the study area and reaches a maximum of 650 m metres towards the upper part of the continental slope. Elevation is divided into seven classes, which are described in Table 1. Class E1 (0 – 100 m) and class E7 (600-700 m) cover the smaller portion (~ 8.2%) of the total area investigated. The rest of the study area is distributed homogeneously among the other classes. Class E3 (200-300 m) covers the largest area (22%) of the investigated slope (Fig. 4a).

The slope gradient (in degrees) of the topographic surface is shown in Fig. 4b. The class limits were defined considering particular conditions of the continental slope, which is very smooth offshore Espírito Santo. Concerning the classification of the slope gradient variable, we did try diverse combinations of classes. Hence, we classified the slope gradient in eight distinct classes in order to discriminate the physical characteristics of the slope (see Table 1). Class S2 represents the bulk of total area investigated (43.5%) and has slope gradients between 1 and 2°. Class S1 represents 35.8% of the total area investigated and has a slope gradient of 0 – 1°. Approximated 13% of the study area comprises slope gradients varying between 2° and 3° (class S3). These three classes combined cover 92.1 % of the total area investigated (Fig. 4b).

The spatial distribution of profile curvature is represented in Fig. 4c. Profile curvature directly affects the acceleration or deceleration of mass-flows along a topographic surface. Profile curvature also relates to the convergence and divergence of mass-flows across a surface (Menno-Jan, 2013). Hence, this factor reflects the change in slope angle, and chiefly controls the change of velocity of mass flows transported down a continental slope (Clerici et al., 2010). Profile curvature is parallel of the maximum slope (Menno-Jan, 2013) and negative values indicate that the surface is convex upwards at a given cell. A positive profile indicates that the surface is concave upwards in that same cell, whereas zero values indicate that the surface is flat. The classes and the distribution of profile curvature in the study area, for the three classes mentioned above, are displayed in Fig. 4c. The classes are almost equally distributed in Table 1. The class PrC2 occupies a small portion (31.5%) of the study area. The two other classes each occupy ~34% of the study area.

Planform (or plan) curvature is perpendicular to the direction of maximum slope. Positive values of planform curvature indicate that the surface is convex sidewards at a given cell. Negative values indicate the surface is concave sidewards, whereas zero values indicate the surface is flat (Fig. 4d). Planform curvature reflects the changes in aspect angle and controls the divergence (or convergence) of mass flows (Clerici et al., 2010), which is related to the superficial and sub-superficial run-off flow on the slope. The spatial distribution of classes is displayed in Fig. 4d, where it is observed that 46.4% of the study area diverges, and 45.7% converge on the investigated slope, with 7.9 % of this latter being virtually flat (Table 1). The contours lines in Fig. 4d help identifying the forms of the three classes proposed. Both profile and planform curvature are calculate using *ArcGis Sotfware*,

Flow direction is one of the keys to understand surface characteristics and the ability to determine the direction of flow between cells in a raster file (Jenson and Domingue, 1988). The topographic surface is the source of a raster showing flow out of which cell using eight-direction (D8) based model (Jenson and Domingue, 1988). The output raster classes are classified with cardinal direction of the flow.

The two first classes FD1 and FD2 are covering an area of 28.6% and 28.5%, respectively. These values indicate that mass-flows have an east to southeast direction in 57% of the investigated area. In 17.7% of the study area, the flow direction is to the south, as represented by class FD3. This is followed by the northeast-trending class FD8, which occupies 12.1% of the study area. The remaining 8.7% is occupied by mass-flows directed to the north, east and northeast, representing 4.9%, 2.5% and 1.3% of the study area, respectively (Fig. 4e).

The final flow accumulation raster reflects the accumulated weight of all cells that are flowing into each downslope cell. In case of concentrate flow, the cells with high flow accumulation may indicate preferential streams channels, in opposite when flow accumulation is 0, it surely indicates local topographic highs (Jenson and Domingue, 1988). Flow accumulation is classified into six logarithmic classes that are represented spatially in Fig. 4f. The class FA3 covers the greatest percentage of the study area with a 41.5% coverage. This is followed by class FA1 with 22.4%. Classes FA2 and FA4 cover 16.2% and 15.2%, respectively. The last two classes, FA5 and FA6 cover together less than 5% of the total area.

The slope over area ratio calculates the ratio of the slope to the specific catchment area or contributing area for each pixel, works as a variable proxy that reflects moisture retention, surface saturation zones and soil water contents. The final map is classified in a logarithmic scale into fixed classes, as represented in Fig. 4g. Class SAR4 is observed in 45.8% of the study area, followed by class SAR3 with 33.6% and SAR2 with 15.7%. Class SAR1 and SAR4 occupied, respectively, 3.2% and 1.7% of the study area, Fig. 4g.

3.3. Mass-transport deposits

The interpretation of the four MTDs in the study area followed previously-established criteria to describe the internal character of remobilized material (e.g. Hampton et al., 1996, Frey-Martínez et al., 2006, Moscardelli and Wood, 2008, Bull et al., 2009, Gamboa et al., 2010, Omosanya and Alves, 2013). Internal reflections in the four MTDs show chaotic stratigraphy and imbricated blocks (e.g. Frey-Martínez et al., 2006). Their basal surfaces are shown as a high-amplitude seismic reflections below the chaotic reflections that form the MTDs (Frey-Martínez et al., 2006). The top of the MTDs is marked by a continuous high-amplitude reflection that overlies chaotic internal reflections (Fig. 3c).

The four MTDs mapped in this work exhibit variable areas, volumes and slope locations, but the thickness of the remobilized material is quite uniform among all MTD population (Table 2). The location of the MTDs in the continental slope of Espírito Santo are shown in Fig. 5 together with the areas of each MTD later considered in models 1 to 3. For model 1, the total unstable area on the continental slope is about 133.8 km^2, i.e. 17.7% of the total study area. In model 2, the unstable area considered is 30.2 km^2, 4% of the total area. Model 3 considered an unstable area of 11.1 km^2, which corresponds to 1.47% of the total area (Table 3).

3.4. Data limitations of 3D seismic data

The dataset used for the application of the proposed modelling strategy has limitations that need be considered in this sub-section. We used as input a high-resolution 3D seismic volume, which is considered an advantage in terms of accuracy and true imaging of geologically significant features. However, when 3D seismic data are converted into GIS there are uncertainties related to the conversion process, and from the fact that some geomorphologic features can be smoothed during this same conversion. The absence of well data in the basin was also an important limitation in our analysis. ODP Site 516 located in the Santos Basin (Fig. 1) was used to convert the data from two-way-travel-time (TwTT) to true depths in metres below the sea floor. Despite the latter ODP site, there was no sufficient spatial information to create geologic layers for modelling proposes.

The MTD inventory in this work thus comprises four slope movements, which were considered valid for the purposes of this analysis. Despite the fact that this inventory is not large enough for data partition, it is nonetheless used to build the predictive model and to validate it (success-rates), providing us the data goodness of fit to the model. As the population of MTDs is relatively small in the study area, the different MTD typologies are not considered into the models and the four MTDs were entered in the same model. Although the MTDs are different in size and volume, we assume the mechanism of rupture and propagation are the same for the 4 inventoried MTD, which is a reason to not separate the inventory. This limitation in the population of MTDs will be under discussed later.

4. GIS modelling

4.1. Mapping of terrain units

The evaluation of the likelihood of mass movements in a given area requires a preliminary selection of suitable terrain units (TMUs). These TMUs refer to a surface portion of the study area containing a set of ground conditions that differ from adjacent units across recognisable boundaries (e.g. Hansen, 1984, van Westen et al., 1997).

The mapping of TMUs usually depends on the scale(s) that better represent the investigated phenomena. From a vast selection of terrain map unit categories (e.g. unique condition units, slope units, geo-hydrological units and topographic units) we used grid cells, which are preferentially used in GIS models. The study area is divided into regular areas (cells) with a predefined size, which became the mapping units of reference (Chung

and Fabbri, 1999, Clerici et al., 2002, Remondo et al., 2003). To each grid cell was given a value for each predisposing factor taken in consideration (e.g. slope gradient, curvatures). Each predisposing factor was computed into a raster file with a given cell size. The main conceptual limitation of grid cells is associated with the representation of continuous geological and morphological forms in a discrete way, as well as the representation of linear and area features - such as geological boundaries, landslide deposits, lithological units - using cells of predefined shapes and sizes (Guzzetti, 2005).

For the present analysis, we chose a set of predisposing factors that can be computed into GIS in a raster format. Due to the size of the study area and mapped MTDs, terrain units (pixels) were fixed at 50 m in five of the seven predisposing factors. The exceptions were the profile and planform curvature, which were first computed with a pixel size of 250 m and subsequently converted into 50 m pixels for modelling.

4.2 Informative Value

In terms of modelling, the predisposing factors are named as independent variables while the MTD inventory is considered in the models as dependent variables.

The Informative Value (IV) is a bivariate statistical method used to weigh each class of variables proposed (Yin and Yan, 1988). It describes quantitatively the relationship between each class of an independent variable (*Xi*) and a set of instability events on slopes through individual scores obtained by Equation 1.

(Eq. 1)

$$IV_i = 1n\left(\frac{S_i / N_i}{S / N}\right)$$

with IV_i – Information value of variable; S_i – Number of pixels with instability events within variable X_i; N_i – Number of pixels with variable X_i; S – Total number of pixels with instability events; N – Total number of pixels of the study area.

In Equation 1, the term *S/N* is the *a priori* probability. It is the probability for each pixel to contain an MTD without considering the independent variable. In parallel, S_i/N_i is the conditional probability; it is the probability of an instability event to occur given the presence of variable X_i. A negative IV_i means that the presence of the variable is favourable to slope stability. A positive IV_i indicates a relevant relationship between

the presence of the variable and MTDs distribution; the higher the score, the stronger the relationship (Yin and Yan, 1988). An IV_i equal to zero means no clear relationship between the presence of the considered variable and the occurrence of MTDs.

The classes of each independent variable not containing MTDs have a conditioned probability of zero. In this case, IV cannot be obtained considering the log transformation in Equation 1, and therefore IV_i was forced to be equal to the lowest IV_i computed for classes of the corresponding independent variable. This procedure does not interfere with the computation of the models. The final models are calculated based on the following equation:

(Eq. 2)

$$Ij = \sum_{i=1}^{n} Xji.Ii$$

Where:

n - number of variables; Xji - either 0 if the variable is not present in the pixel j, or 1 if the variable is present. The IV was calculated using three different partitions of the same MTD inventory such as:

1. Model 1: includes the total area of MTDs.
2. Model 2: includes 1/3 of the total length of the mapped MTDs.
3. Model 3: includes half of the area used in model

4.3 Model validation: Success-rate curves

The performance of the predictive models was assessed through the computation of success-rate curves (Fabbri et al., 2002). Success-rates curves are based on the comparison between the final model and the spatial distribution of MTDs, and they are used to weigh the predictive variables expressing the goodness of fit of the MTDs used and the final model (Chung and Fabbri, 2003).

Success-rate curves are prepared by plotting the cumulative percentage of the area most likely to fail (starting from the highest probability values towards the lowest) on the horizontal (x) axis, and the cumulative percentage of corresponding MTDs area on the vertical (y) axis. The steeper the curve, the more capable the model is to describe the distribution of MTDs in a given study area. The steepness of the curve also depends on the spatial distribution of instability events in the investigated area(s). In a situation when a large portion of the area is covered by instability, it is still possible to get steep curves (Chung and Fabbri, 1999).

The favourability values obtained for each pixel were sorted in descending order. Additionally, an Area Under the Curve (AUC) analysis was computed for each success-rate curve so one can quantify the performance of each model and compare results for the different success-rates. The higher is the AUC value, the better is the model (Bi and Bennett, 2003, Blahut et al., 2010, Pereira et al., 2012, Guillard and Zêzere, 2012) the absolute AUC value is given by:

(Eq. 3)

$$AUC = \sum \left[\left(x_{i+1} - x_i \right) \frac{y_{i+1} + y_i}{2} \right]$$

where x is the percentage of the study area predicted as susceptible by descending order, and $\boldsymbol{y}$ is the percentage of correctly classified landslide area belonging to the validation group.

4.4 Sensitivity analysis

A sensitive analysis of the variables was performed after the AUC calculations in order to understand which combination of factors most contributes to trigger unstable areas on the Espírito Santo continental slope. Each independent variable (predisposing factors) was crossed autonomously with the MTD inventory, generating an individual model for each variable. Thus, each individual model was validated by building a success-rate and respective calculation of AUC for each independent variable in the model. The results were ordered by growing range to rank and compare the importance of each variable into the final model. The ranking mentioned above was also taken into consideration throughout the sensitivity analysis.

The finally sensitivity analysis was computed by adding a systematic way through the introduction of a new variable (V) considering the AUC obtained when crossing which variable independently. The models (M) obtained using from 2 to 7 predisposing factors, whereby $M_2 = V_1 + V_2$; $M_3 = V_1 + V_2 + V_3$; $M_4 = V_1 + V_2 + V_3 + V_4$) and $M_n = f\ (V_1 + V_2 + V_3 + V_4 + \ldots V_n)$. For each model obtained, AUC was calculated so to understand which variable combination obtains better predictive capacity (e.g. Guzzetti et al., 2006, Zêzere et al., 2008).

5. Results

5.1 Multicollinearity diagnosis

The multicollinearity diagnosis is summarized in Table 4. Based on the literature is considered multicollinearity when VIF is > 2 and TOL <0.2, whereby all the variable used in the models where considerably under of the stabilised minimums values. Slope over area ratio is presenting the highest value (1.70 VIF and 0.670 TOL), however we considered these values suitable to enter in the models since they were within the thresholds considered above.

5.2 Weighting of variables

The weighting of variables for the evaluation of favourability scores for MTDs is calculated applying the Informative Value (IV) bivariate statistical method, the methodology of which is described before. The weighting is prepared using three different partitions for the same MTDs inventory: 1) model 1, using the total area of MTDs inventory; 2) model 2 – using 1/3 of MTDs total length and; 3) model 3 – using half of the length in used in model 2. The area that each class occupies, in percentage, is shown in Table 1. Informative values for each class of each variable considering each model are summarized in the Table 5.

5.3 Informative Value Scores (IV)

Informative Value scores obtained from the three susceptibility models (models 1 to 3) are summarized in Table 5. In bold are highlighted the highest favourability scores for the occurrence of MTDs for each variable. The values in red are classes for which it was not possible to compute IV scores due the absence of MTDs pixels ($Si = 0$), a caveat resulting from its logarithmic transformation. The classes with higher IV scores i.e., that contribute more for the occurrence of MTDs in the study area, differ as a function of the total area considered in the three models performed (models 1 to 3).

In model 1 we considered the total length (and area) of MTDs in the study area and, based on the IV scores obtained, it is possible to state that the occurrence of MTDs was conditioned by local factors. Local factors of importance include an elevation between 100 – 300 m (namely elevation classes between 100 – 200 m), slope gradients between 1 and 2 degrees, and concave slope areas in both profile and plan curvature. Slopes that are most prone to the occurrence of MTDs are those flowing to SW and, secondarily, to S. In this

model, the critical flow accumulation for the occurrence of MTDs occurs in the class >1000 and the most MTD prone slope over area ratio of ~0 (Table 5).

Model 2 was performed using 1/3 of the total MTDs length. Favourable conditions for the occurrence of MTDs occurrence change in model 2 when compared with model 1, as initially expected. In this case, the ideal conditions for the occurrence of MTDs are elevation ranging from 500 to 600 m and, to a lesser extent, elevation ranging between 300 and 400 m. Slope gradient ranges from 1 to 6 degrees, with the interval between 2-6° being the most favourable to the occurrence of MTDs. Concave slopes are prone to generate MTDs when considering the profile and plan curvature, as also recorded in model 1. The critical flow direction is S and SE, although NE-dipping slopes also appear as favourable to the occurrence of MTDs. The flow accumulation most likely for the occurrence of MTDs is >1000 and, to a lesser extent, class 100 – 1000. Regarding slope over area ratio two classes are highlighted in model 2: 0-0.00001 and 0.00001 to 0.0001 (Table 5).

Model 3 used only half of the length of the MTDs considered in model 2, but results show that preferential conditions for the occurrence of MTDs are similar to model 2. In model 3, perfect conditions for MTD occurrence are elevation between 500 and 600 m and to a less extent, elevation between 300 and 400 m. Slope gradient plays a major role in model 2, particularly within the class ranging between 2° and 6°. As with models 1 and 2, slope curvatures most prone to MTD occurrence are concave and their flow directions are essentially S and SE. A Flow accumulation class >1000 is the most favourable, while the class 0 is the most favourable regarding the slope over area ratio (Table 5).

6. Data integration and predictive maps

Predictive maps are the final output resulting from the integration of all the analytical steps previously described. Predictive maps represent the spatial distribution of the susceptibility of continental slopes for the occurrence of MTDs, considering the three models developed. The maps presented are computed based on the seven predisposing factors (variables) previously described. Thus, Fig. 6a was computed using the total area of MTDs, as considered in model 1. Fig. 6b was computed with inventory used in model 2. Finally, Fig. 6c is presented based on the outputs of model 3. The three models show a non-classified legend, sorted in descending order of favourability values. From a preliminary visual observation, there are clear differences

between the three maps. Nevertheless, one can observe the predominant impact of the same variables - elevation, slope gradient, profile curvature, flow direction, flow accumulation and slope over ratio - in the three models.

6.1 Validation – Success-rates

The AUC values range from 0-1, considering that the quality of the model increases towards a value of 1. Models showing an AUC of 0.75 are "acceptable", > 0.80 "very good" and >0.90 are considered "excellent" (Guzzetti, 2005). The success-rate curves for models 1 to 3 are displayed in Fig. 7. As previously mentioned, the success-rate measures the goodness of fit. Assuming the model is correct for the analysed area, model 1 (dark blue line Fig. 7) was performed using the total area of the mapped MTDs and shows the lower goodness of fit. For model 1, AUC is 0.657 (66%). In model 1, 30% of the area classified as most favourable to the occurrence of MTD validates 50% of the MTDs. In order to validate all the MTDs is necessary to consider 90% of the study area as it is shown in Fig. 7 where is visible that curves loose gradient.

Considering model 2 (light blue line in Fig. 7), AUC shows the model to perform better in comparison to model 1. The goodness of fit for model 2 is 0.747 (75%). Considering 50% of the area classified as most favourable to the occurrence of MTDs, model 2 is valid for around 85% of the MTDs area. Yet, the whole of the MTD area is only validated when 90% of the study area is reached.

The model 3 presents the highest goodness of fit, with an AUC of 0.862 (86%). The 30% of the area classified as most favourable to the occurrence of MTDs validates 90% of the MTD area, reaching a 100% validation with 55% of the total area.

Through the AUC's plots is observed that model 3 obtained the highest performance of the three models with 0.862 (Fig. 7). Considering the classification of Guzzetti (2005), this value plots within the "very good" class. Model 2 obtained 0.747 of AUC, which can be classified as "acceptable", whereas model 1 recorded an AUC of 0.657, which is below an acceptable class.

6.2 Sensitivity analyses

Sensitivity analyses allowed us to outline which predisposing factors are key to explaining the spatial distribution of a dependent variable (e.g. the MTD). Sensitivity analyses assess the weight of different MTD

predisposing factors within a statistically-based model. Therefore, model 3 was chosen in this sub-section to run a sensitivity analysis, as it obtained the highest AUC value (0.862) from the three built models.

Table 6 shows the hierarchy of predisposing factors with the highest contribution to the occurrence of MTDs in the study area. The hierarchy is selected through the AUC values for success-rates ran independently for each predisposing factor (Fig. 8). Through these analyses, we observe that elevation is the predisposing factor which most influences model 3, with 0.832 of AUC. It is followed by slope gradient, showing 0.616 of AUC and the flow direction with 0.584 (Table 6). At the bottom of the hierarchy appears a slope over area ratio showing an AUC of 0.493. Observing the curves in Fig. 6 is clear the contribution of the variable elevation where 35% of the total area validates almost the entire unstable area.

The results obtained in the sensitivity analysis demonstrate that the independent variables considered do not correlate precisely with the distribution of MTDs. This is best demonstrated by the AUC range obtained, which varies from 0.493 (Slope over area ratio) to 0.832 (elevation). The ranking expressed in Table 6 was thus used to define the relative importance of the MTD predisposing factors that support the model. Successive models were performed adding one additional variable to the model at each step following the raking previously archived.

The quality of MTDs predictive model demonstrates a slight tendency to improve with increasing numbers of variables, as shown by the AUC values in Table 7. This is particularly true until the model is run with 4 variables, from which moment a maximum AUC of 0.861 is achieved. After that, the increment of variable does not increase the predictive performance of the model 3 (Table 7, Fig. 9). Success curves represented in Table 7 show that all models tend to behave similarly, whereby if we consider 30% of the area classified as most favourable to the occurrence of MTDs, the predicted results are similar in all models with a different set of variables (90%). This behaviour demonstrates the low sensibility of MTDs prediction to the increasing number of MTDs predisposing factors considered in our models.

7. Discussion

7.1 Topographic surface, predisposing factors and modelling

The rationale for the work presented in this paper was based on landslide susceptibility analyses undertaken onshore, which are part of the conceptual modelling of geological risk (e.g. van Westen et al., 1997, Guzzetti et al., 2006, Thiery et al., 2007, van Westen et al., 2008, Blahut et al., 2010, Guillard and Zêzere, 2012, Pereira et al., 2012). Based on the conceptual model of risk, the existence of a topographic surface is crucial as a proxy of onshore Digital Terrain Models (DTM), from where we can compute a set of derived variables that can be used in GIS to assess slope movements. Therefore, the following step in our analysis was to map in seismic data a palaeo-surface that could reproduce seafloor topography, and could be used as a DTM. This concept was previously applied to marine studies (e.g. Micallef, 2011).

The topographic surface mapped in this work was chosen based on two key aspects. The first was the necessity of mapping a high-amplitude, regionally significant seismic reflection that covers the entire study area. Secondly, we thought appropriate to map all different MTD bodies just above the interpreted seismic reflection (topographic surface). In our methodology, the topographic surface mapped thus becomes crucial to the analysis as it must represent seafloor topography before the instability event occurred. In other words, it must not only reflect the morphology associated with slope instability but also the terrain attributes which were present before the occurrence of the MTDs.

In onshore studies, a DTM is used to analyse the topographic features that are favourable to slope instability. In a previous work, Clerici et al. (2010) discussed a better approach for susceptibility studies, pointing out that some factors such slope angle, aspect or curvature may be modified by the occurrence of slope instability events, so the morphology present when the topographic/bathymetric/seismic survey is acquired can be substantially different from the pre-instability conditions. In such a case, some authors suggested and agreed that the (predisposing) factors should be acquired in undisturbed areas, immediately surrounding the unstable areas (Clerici et al., 2002, Clerici et al., 2010) unless the morphometric parameters in those areas do not relate at all to the reality of pre-failure slope conditions. In 2007, Micallef et al. pointed out four morphometric maps used in the Storegga Slide using GIS terrain delivery attributes. The criteria to choose the variables to use into the bivariate is based on the mentioned studies that had proven to be capable to determinate area where the slope movement are more prone to occur. The variables are originated from exclusively the interpreted seismic volume - local information such as lithology were insufficient to interpolate

and create a map containing its spatial distribution, due the inexistence of data wells over the study area, which is a pitfall for this study.

The models in this paper were computed using three different areas of the same inventory. Clerici et al. (2010) pointed out that this kind of studies can identify the conditions under which the instability events are generated. This way, the favourability analyses had to be restricted to the areas from where the mass movement originated, i.e. the rupture zones. Other authors (Chung and Fabbri, 2005, Guillard and Zêzere, 2012) stressed this same limitation, but concluded that modelling the favourability of slopes to the occurrence of mass movements using different landslide input data (e.g. the complete landslide area or the landslide depletion area) does not affect the final results. To confirm this latter postulate, the model used three different MTD zones obtained from the same inventory. Based on this, the reason to model three distinct areas was to try getting close of what is believed to be the rupture zone and consequently to the area where the movement starts even without knowing exactly how much displacement it can present. The use of the total area (model 1) is not considered as the most correct approach for the majority of the authors because the predisposing factors are estimated also for the accumulation zone, which is affected by the arrival of depleted material from up-slope source areas. In this case, the conditions present in the accumulation zone are erroneously considered to be prone to sliding (Clerici et al., 2010).

Acknowledging the latter caveat, the data inventory was reduced to 1/3 of the total length in model 2, getting close to excluding the accumulation zones of the interpreted MTDs. This improved substantially the quality of model 2 when compared to model 1. However, the best performance was achieved by model 3 by constraining the probable rupture zone to half of the length considered in model 2. A sensitivity analysis was undertaken crossing each variable (predisposing factors) individually with the inventory of MTDs used in model 3 (which obtained the best predictive capacity), and the computation of success-rates and AUCs for each individual variable (Chung and Fabbri, 1999, Zêzere et al., 2008, Blahut et al., 2010, Pereira et al., 2012). The results demonstrated that the independent variables considered do not contribute equally to explain the distribution MTDs in the study area, showing AUCs ranging from 0.493 to 0.832 (Table 5). Moreover, according to the AUC records, elevation and slope gradient are the variables that better correlate with the spatial occurrence of MTDs, showing AUCs of 0.832 and 0.616, respectively. Elevation is not often used as a predisposing factor; yet some authors have considered elevation as a predisposing factor valid enough to be included in the models (e.g. Remondo et al., 2003, van Westen et al., 2008). In this analysis, elevation was

included on all the modelling sets, and is revealed as the variable with higher prediction performance in model 3. Slope gradient is generally the variable that most contributes to explaining slope instability (e. g. Remondo et al., 2003, Piedade et al., 2010, Pereira et al., 2012), but its recorded in this work as showing less predictive capacity when compared to elevation (Table 5).

The fact that elevation is the variable that most contributes to the models can be related to multiple factors such as local geology - different lithological facies that can be present in different elevations to favour to the occurrence of MTDs, which cannot be proved due to missing detailed lithological data. Salt tectonics is another important phenomenon playing an important role in shaping of the Espírito Santo Basin. Overburden accommodation space is responsible by the sediment remobilisation and deposition, which can be more frequent in specific elevation sets due the location of the fault or week sedimentological layers (Piedade, 2016). Another reason that can explain the results obtained for the elevation variable is the influx of sediments coming from the shelf edge, acting as an 'external' force on the slope or constituting a weak layer prone to glide when triggered by an external factor. Hühnerbach and Masson (2004) documented, in the western Canary Islands, that the greatest number of submarine landslide headwalls occurs on the mid-slope, with a peak at 1000 – 1300 m water depth, rather than at the shelf edge or upper slope as one might be expect. The results of predictive models obtained in this study for the Espírito Santo Basin are in line with Hühnerbach and Masson (2004) findings - the head scarp of the interpreted MTDs are located roughly at the same depth (Fig. 1). The last explanation that can be pointed out is related to a marked structural control of the salt and raft tectonics as pointed out at Piedade and Alves (2017).

Onshore, slope gradient exerts a significant influence on mass movement's distribution. Indeed slope gradient or slope angle has been proved to be the predisposing factor that more contribute to the occurrence of mass movements onshore (Zêzere et al., 2008, Piedade et al., 2010, Pereira et al., 2012, Guillard and Zêzere, 2012). In the three models developed in the work, slope gradient is the second variable that contributes more to the predictive models (Table 6). Compared to elevation, the AUC of slope gradient is significantly reduced. Nevertheless, in the literature slope gradient is not the factor considered the most important for the occurrence of MTDs in offshore environments. Masson et al. (2006) refer that the largest submarine landslides occur in areas where specific aspects of the local geology and morphology are placed together to trigger slope failure. Continental slopes on which mass movements occur are typically of low gradients (1° to 5°) and gentle topography (Wilson et al., 2004, Hühnerbach and Masson, 2004, Masson et al., 2006). In the models presented

in this work, the slope gradient where most MTDs occur varies between 1° to 6°, and can be considered of low gradient. Model 3 achieved the best goodness of fit (Fig. 7), in which the headwall scarp domain of the MTD has a slope angle of 6º. However, when the others two models are considered the favourability scores for slope gradient are extended to areas of lower slope gradients. This is explained by the fact that the models with larger area and length (models 1 and 2) are already modelling part of the run-out areas of the MTDs (Model 2) or even the total area of run-out (model 1).

Flow direction appears as the third most crucial parameter in the three models. Considering Table 6, the flow direction variable increases the predictive capacity of the models However, adding more variables to the models does not increase its predictive rate, meaning that the set of variables including elevation, slope gradient and flow direction is the most appropriate to assess the spatial distribution of MTDs in the study area.

The other variables used in the model are showing a very little contribution for the final prediction values. It still clear that Elevation provides the greater contribution by the curve trend. The slope over ratio does not give any contribution to the model, been the worse variable within model 3.

The ranking of variables was performed to understand which variables add more weight to the final model, but also to understand which are the best variable combinations. The capacity of the predictive models does not tend to improve with the increment on the number of variables within the model, as showed by the AUC distribution in Table 7. Thus, the models performed using four variables (elevation, slope gradient, flow direction and plan curvature) show the highest AUC (0.861). The results mean that the increment of variables in the MTD predictive models do not necessarily generate better success-rates.

Knowing that, the results obtained by the validation exercise match the published literature. The validation exercise in this paper does not necessarily represent an improvement on the predictive capacity of the models, but success rates and AUC analyses help to discriminate the importance of each variable within the models considered in slope stability assessments undertaken using 3D seismic data. Despite the valid results in this work, we need to point out that due the small population of MTDs, the models presented here did not separately consider the different types of MTDs identified in the study area. In onshore studies, different types of slope movements have been modelled separately based on the assumption that different slope movements are caused by different natural conditions (van Westen et al., 2008, Pereira et al., 2012).

7.2 Applicability of the method to submarine slopes

Theoretically and practically, the methodology proposed in this work has positive results on onshore studies, which has been extensively used and included in land management, urban planning and natural hazards prediction (Carrara et al., 1999, van Westen et al., 2003, Malamud et al., 2004, Pereira et al., 2012). Yet, the applicability of this method to submarine environments cannot simply be taken for granted. To apply statistical methods used on land to submarine environments, some assumptions must be made when collecting and integrating basic morphological data. This work proposes the acquisition of topographic/morphological information through the mapping of palaeosurfaces represented as high-amplitude seismic reflections on 3D seismic data. The results confirm that the methodology adopted constitutes a valid approach; it nevertheless needs to consider the resolution of the interpreted seismic volumes. Even when using high resolution seismic, topographic details can be partly lost by incorrect processing techniques and seismic artefacts (Marfurt and Alves, 2015) or simply by seismic vertical and horizontal resolution. The statistical bivariate analysis showed can be used in the assessment of offshore slopes and it may have better results if applied to seafloor data.

Micallef et al. (2007) proposed the applicability of subaerial quantitative geomorphological techniques to submarine environments, opening an important research field in the direction of the rational and methodology presented in this paper, as well as, Dabson et al. (2016), recently discussed the use of geomorphologic features into multivariate submarine slope assessment models. Nevertheless, the work presented by Borrell, et al. (2016) used geologic features, as seafloor composition and fault for susceptibility assessment offshore, presenting a susceptibility map supported by this essential data, but not always available. It is also mentioned as a pitfall the limited available control factor maps. By taking into consideration the know-how derived from these studies, and together with the compilation of predictive models to explained landslides susceptibility, that this work took a step further by applying it to palaeo-MTDs offshore Espírito Santo, SE Brazil. The main advantage of the methodology is the possibility of understanding which variables (or predisposing factors) are capable of better predicting the location of future slope instability events. Which can be complete and add more valid information to the studies which only considered geologic features when in the future will be considered the models of palaeo-slopes.

Geographic information Systems (GIS) are very suitable for indirect landslide hazard assessments, in which all possible terrain factors contributing to slope instability are combined within a landslide inventory map using data integration techniques (van Westen et al., 2003). In addition, Chung and Fabbri (1999) developed statistical procedures and denominated it as 'predictive modelling', applying favourability functions on individual parameters. Using this statistical methods, terrain units or grid cells can be adjusted to new values representing the degree of probability, certainty, belief or plausibility that the respective terrain units or grid cells may be subject to a particular type of landslide in the future. van Westen et al. (2006) pointed out several drawbacks of this approach. One of these drawbacks is the fact that most methods simplify the factors that condition landslides by using only the variables that can be relatively easily mapped in an area, or derived from a DTM. Another problem also identified in the literature is related to the fact that each instability event (and type) will have its own set of predisposing factors and should be analysed individually. Different typologies need to be modelled separately. In this study, due the restriction of MTDs population (four cases), the models were computed not taking it into consideration, which can create more uncertainties to the results. For the same reason, the models were validated through the success-rate (same inventory to model and to validate), which assess the goodness of fit of the MTD to the final model. In case of larger inventory, the predictive-rates that use a different inventory to model run and validation, the result are more accurate in predicting where MTDs will occur in the future, under the same geomorphologic conditions.

The bivariate statistical models, including the Informative Value presented in this paper, still limited from geomorphological point of view, even when applied to onshore studies. Its expert dependency is very high because its good performance strongly depends from the inventory quality. When applied to offshore the uncertainties are even higher, because it still dependent of the expert knowledge about geomorphologic process but also from seismic resolution and to produce a reliable mass movement inventory, which is crucial to model quality. This fact, is also important because statistical models are very sensitive to the number of cells (pixels, in this case) that overlap the variables, once again responding to a quality of the inventory, which should have as must movements as possible and separated by typology.

8. Conclusions

The primary conclusion is that the new methodology presented within this study can be positively applied to offshore slope instabilities, as the goodness of fit of the models was favourable. However, detailed observations about the best ways to apply this method need to be point out:

- The technique of mapping a depositional surface from a 3D seismic survey is a valid method and can be used as topographic database. The horizon needs to be a relatively high-amplitude reflection and should be possible to follow throughout the study area.

- The data that can be extracted from a seismic volume must be carefully considered. Most mapping techniques are unable to extract very detailed morphological features, due the limitations in seismic resolution.

- The bivariate statistic Informative Value (IV) method was revealed to be applicable to submarine environments. It was observed that models respond differently according the type and detail of MTD data provided to the model.

- The three models compiled were assessed via the analysis of success-rates and computing the AUC. The assessment reveals that model 3, which contains the MTDs area of which is believed to be the closest of the rupture zone, shows a highest AUC of 0.86. According (Guzzetti, 2005), this value can be classified as "Very good".

- The model performed using the set designed by model 2 revels an AUC of 0.747, which following the classification above mentioned is on the lower threshold considering "acceptable". The model performed using the total MTD area (model 1) reveals the poorest AUC (0.657). The results fit the expectations that modelling using the entire MTD body does not exactly reflect the predisposing factors at the rupture zone, where MTDs started.

- Sensitivity analysis performed to the model which obtained the highest AUC (model 3), indicate that elevation and slope gradient are the most important variables in MTD initiation.

- Elevation is the variable that most contributes to the explanation of the MTDs in the study area, which is clear by marking the zonation of MTD occurrence in the predictive models.

Acknowledgments

We are thankful to *CCG* for the permission to publish this data. We also thanks *Schlumberger* for providing *Petrel interpretation software*, *Exprodat GIS for Petroleum* for the license of *Data Assistant software and ESRI* for providing *ArcGis License* itself. Aldina Piedade was supported in her PhD by FCT-Portugal (SFRH/BD/79052/2011). She is now a PostDoc researcher at CISUC, Universidade de Coimbra, Portugal. The authors acknowledge the two anonymous reviewers for their constructive comments. Dr Michele Rebesco is acknowledged as MG editor and for his appreciable comments.

References

ALVES, T. M. (2015). Submarine slide blocks and associated soft-sediment deformation in deep-water basins: A review. *Marine and Petroleum Geology, 67*, 262-285.

AlVES, T. M., & LOURENÇO, S. D. N. (2010). Geomorphologic features related to gravitational collapse: Submarine landsliding to lateral spreading on a Late Miocene–Quaternary slope (SE Crete, eastern Mediterranean). *Geomorphology*, 123(1), 13-33.

BAI, S. B., WANG, J., LÜ, G.-N., ZHOU, P. G., HOU, S. S., & XU, S. N. 2010. GIS-based logistic regression for landslide susceptibility mapping of the Zhongxian segment in the Three Gorges area, China. *Geomorphology, 115*(1), 23-31.

BARKER, P. F., BUFFER, R. T. & GOMBÔA, L. A. 1993. A seismic reflection study of the Rio Grande Rise. *Barker, P. F., Carlson, R. L., Hohnson, D. A. (Eds.), Initial Reports of the Deep Sea Drilling Program. Government Printing Office, Washington, DC.***,** 953 - 976.

BI, J. & BENNETT, K. P. 2003. Regression Error Characteristic Curves. Proceedings of the 20th International Conference on Machine Learning (ICML-03), Washington, DC, 43-50.

BLAHUT, J., VAN WESTEN, C. J. & STERLACCHINI, S. 2010. Analysis of landslide inventories for accurate prediction of debris-flow source areas. *Geomorphology,* 119**,** 36-51.

BORRELL, N., SOMOZA, L., LEÓN, R., MEDIALDEA, T., GONZALEZ, F. J. & GIMENEZ-MORENO, C. J. (2016). GIS Catalogue of Submarine Landslides in the Spanish Continental Shelf: Potential and Difficulties for Susceptibility Assessment. In G. Lamarche, J. Mountjoy, S. Bull, T. Hubble, S. Krastel, E. Lane, A. Micallef, L. Moscardelli, C. Mueller, I. Pecher & S. Woelz (Eds.), *Submarine Mass Movements and their Consequences: 7th International Symposium* (pp. 499-508). Cham: Springer International Publishing.

BULL, S., CARTWRIGHT, J. & HUUSE, M. 2009. A review of kinematic indicators from mass-transport complexes using 3D seismic data. *Marine and Petroleum Geology,* 26**,** 1132-1151.

CARRARA, A., GUZZETTI, F., CARDINALI, M. & REICHENBACH, P. 1999. Use of GIS Technology in the Prediction and Monitoring of Landslide Hazard. *Natural Hazards,* 20**,** 117-135.

CHUNG, C. J. & FABBRI, A. 2003. Validation of Spatial Prediction Models for Landslide Hazard Mapping. *Natural Hazards,* 30**,** 451-472.

CHUNG, C. J. & FABBRI, A. G. 1999. Probabilistic prediction models for landslide hazard mapping. *Photogrammetric Engineering and Remote Sensing,* 65-12**,** 1389-1399.

CHUNG, C. J. F. & FABBRI, A. G. 2005. Systematic Procedures of Landslide Hazard Mapping for Risk Assessment Using Spatial Prediction Models. *Landslide Hazard and Risk.* John Wiley & Sons, Ltd.

CLERICI, A., PEREGO, S., TELLINI, C. & VESCOVI, P. 2002. A procedure for landslide susceptibility zonation by the conditional analysis method. *Geomorphology,* 48**,** 349-364.

CLERICI, A., PEREGO, S., TELLINI, C. & VESCOVI, P. 2010. Landslide failure and runout susceptibility in the upper T. Ceno valley (Northern Apennines, Italy). *Natural Hazards,* 52**,** 1-29.

DABSON, O. J. N., BARLOW, J., & MOORE, R. 2016. Morphological Controls on Submarine Slab Failures. In G. Lamarche, J. Mountjoy, S. Bull, T. Hubble, S. Krastel, E. Lane, A. Micallef, L. Moscardelli, C. Mueller, I. Pecher & S. Woelz (Eds.), *Submarine Mass Movements and their Consequences: 7th International Symposium* (pp. 519-528). Cham: Springer International Publishing.

DAI, F. C., LEE, C. F. & NGAI, Y. Y. 2002. Landslide risk assessment and management: an overview. *Engineering Geology,* 64**,** 65-87.

FABBRI, A., CHUNG, C., NAPOLITANO, P., REMONDO, J. & ZÊZERE, J. 2002. Prediction rate functions of landslide susceptibility applied in the Iberian Peninsula. *Risk analysis III, series: management information systems,* 5**,** 703-718.

FIDUK, J. C., BRUSH, E. R., ANDERSON, L. E., GIBBS, P. B. & ROWAN, M. G. 2004. Salt deformation, magmatism, and hydrocarbon prospectivity in the Espirito Santo Basin, offshore Brazil. *Salt-Sediment Interactions and Hydrocarbon Prospectivity: Concepts, Applications, and Case Studies for the 21st Century. Houston, Gulf Coast Section Society of Economic Paleontologists and Mineralogists,* 24th Annual Research Conference, 370-392.

FRANÇA, R. L., DEL REY, A. C., TAGLIARI, C. V., BRANDÃO, J. R. & FONTANELLI, P. R. 2007. Bacia do Espírito Santo. *Bol. Geocienc. Petrobras,* 15**,** 501 - 509.

FREY-MARTÍNEZ, J., CARTWRIGHT, J. & JAMES, D. 2006. Frontally confined versus frontally emergent submarine landslides: A 3D seismic characterisation. *Marine and Petroleum Geology,* 23**,** 585-604.

GAMBOA, D., ALVES, T., CARTWRIGHT, J. & TERRINHA, P. 2010. MTD distribution on a 'passive' continental margin: The Espírito Santo Basin (SE Brazil) during the Palaeogene. *Marine and Petroleum Geology,* 27**,** 1311-1324.

GILBERT, R. B., LACASSE, S. & NADIM, F. 2013. Advances in geotechnical risk and reliability for offshore applications. *Geotechnical Safety and Risk IV.* CRC Press.

GLADE, T. & CROZIER, M. J. 2005. A Review of Scale Dependency in Landslide Hazard and Risk Analysis. *Landslide Hazard and Risk.* John Wiley & Sons, Ltd.

GUILLARD, C. & ZÊZERE, J. 2012. Landslide Susceptibility Assessment and Validation in the Framework of Municipal Planning in Portugal: The Case of Loures Municipality. *Environmental Management,* 50**,** 721-735.

GUZZETTI, F. 2005. Landslide hazard and risk assessment – concepts, methods and tools for the detection and mapping of landslides, for landslides susceptibility zonation and hazard assessment, and for landslide risk evaluation. *PhD Thesis. Mathematchinaturwissenschaftlichen Fakultät da Rheinischen Friedrich-Wilhelms,* University of Bonn.

GUZZETTI, F., REICHENBACH, P., ARDIZZONE, F., CARDINALI, M. & GALLI, M. 2006. Estimating the quality of landslide susceptibility models. *Geomorphology,* 81**,** 166-184.

HAMPTON, M. A., LEE, H. J. & LOCAT, J. 1996. Submarine landslides. *Reviews of Geophysics,* 34**,** 33-59.

HANEBERG, W. C., KELLY, J. T., GRAVES, H. L. & DAN, G. 2015. A GIS-based decision-support approach to deepwater drilling-hazard maps. *The Leading Edge,* 34**,** 398-404.

HOUGH, G., GREEN, J., FISH, P., MILLS, A. & MOORE, R. 2011. A geomorphological mapping approach for the assessment of seabed geohazards and risk. *Marine Geophysical Research,* 32**,** 151-162.

HÜHNERBACH, V. & MASSON, D. G. 2004. Landslides in the North Atlantic and its adjacent seas: an analysis of their morphology, setting and behaviour. *Marine Geology,* 213**,** 343-362.

LECOURS, V., DOLAN, M. F. J., MICALLEF, A. & LUCIEER, V. L. 2016. A review of marine geomorphometry, the quantitative study of the seafloor. *Hydrol. Earth Syst. Sci.,* 20**,** 3207-3244.

JENSON, S. K., and J. O. DOMINGUE. 1988. Extracting Topographic Structure from Digital Elevation Data for Geographic Information System Analysis. *Photogrammetric Engineering and Remote Sensing 54 (11)*: 1593–1600

LI, C., WU, S., ZHU, Z. & BAO, X. 2014. The assessment of submarine slope instability in Baiyun Sag using gray clustering method. *Natural Hazards***,** 74 (2), 1179-1190.

MALAMUD, B. D., TURCOTTE, D. L., GUZZETTI, F. & REICHENBACH, P. 2004. Landslide inventories and their statistical properties. *Earth Surface Processes and Landforms,* 29**,** 687-711.

MARFURT, K. J. & ALVES, T. M. 2015. Pitfalls and limitations in seismic attribute interpretation of tectonic features. *Interpretation,* 3**,** 5-15.

MCADOO, B. G. 2000. Mapping Submarine Slope Failures. *Marine and Coastal Geographical Information Systems, London: Taylor and Francis***,** 189-204.

MELO, R., & ZÊZERE, J. L. 2017. Modeling debris flow initiation and run-out in recently burned areas using data-driven methods. *Natural Hazards*, 88(3), 1373-1407.

MENNO-JAN, K. 2013. Map use: reading, analysis, interpretation. *Cartography and Geographic Information Science,* 40**,** 53-54.

MICALLEF, A. 2011. Marine Geomorphology: Geomorphological Mapping and the Study of Submarine Landslides. *Developments in Earth Surface Processes,* 15, 377-395.

MICALLEF, A., BERNDT, C., MASSON, D. G. & STOW, D. A. V. 2007. A technique for the morphological characterization of submarine landscapes as exemplified by debris flows of the Storegga Slide. *Journal of Geophysical Research: Earth Surface,* 112**,** F2.

MOHRIAK, W., NEMČOK, M. & ENCISO, G. 2008. South Atlantic divergent margin evolution: rift-border uplift and salt tectonics in the basins of SE Brazil. *Geological Society, London, Special Publications,* 294**,** 365-398.

MOSCARDELLI, L. & WOOD, L. 2008. New classification system for mass transport complexes in offshore Trinidad. *Basin Research,* 20**,** 73-98.

MOSCARDELLI, L. & WOOD, L. 2015. Morphometry of mass-transport deposits as a predictive tool. *Geological Society of America Bulletin*.

MOSCARDELLI, L., WOOD, L. & MANN, P. 2006. Mass-transport complexes and associated processes in the offshore area of Trinidad and Venezuela. *AAPG bulletin,* 90**,** 1059-1088.

NADIM, F. 2006. Challenges to geo-scientists in risk assessment for sub-marine slides. *Norsk Geologisk Tidsskrift,* 86**,** 351-362.

OMOSANYA, K. D. O. & ALVES, T. M. 2013. Ramps and flats of mass-transport deposits (MTDs) as markers of seafloor strain on the flanks of rising diapirs (Espírito Santo Basin, SE Brazil). *Marine Geology,* 340**,** 82-97.

PEREIRA, S., ZÊZERE, J. L. & BATEIRA, C. 2012. Technical Note: Assessing predictive capacity and conditional independence of landslide predisposing factors for shallow landslide susceptibility models. *Nat. Hazards Earth Syst. Sci.,* 12**,** 979-988.

PIEDADE, A. 2016. *An integrated approach to assess slope instability offshore Espírito Santo, SE Brazil*. PhD Thesis, Cardiff University.

PIEDADE, A. & ALVES, T. M. 2017. Structural styles of Albian rafts in the Espírito Santo Basin (SE Brazil): Evidence for late raft compartmentalisation on a 'passive' continental margin. *Marine and Petroleum Geology,* 79**,** 201-221.

PIEDADE, A., ZÊZERE, J. L., ANTÓNIO TENEDÓRIO, J., GARCIA, R. A., OLIVEIRA, S. C. & ROCHA, J. Generalization of landslide susceptibility models in geologic-geomorphologic similar context. *EGU General Assembly Conference Abstracts,* 2010. 3666.

REMONDO, J., GONZÁLEZ-DÍEZ, A., DE TERÁN, J. & CENDRERO, A. 2003. Landslide Susceptibility Models Utilising Spatial Data Analysis Techniques. A Case Study from the Lower Deba Valley, Guipuzcoa (Spain). *Natural Hazards,* 30**,** 267-279.

RODRÍGUEZ-OCHOA, R., NADIM, F., CEPEDA, J. M., HICKS, M. A. & LIU, Z. 2015. Hazard analysis of seismic submarine slope instability. *Georisk: Assessment and Management of Risk for Engineered Systems and Geohazards,* 9**,** 128-147.

SOETERS, R. & VAN WESTEN, C. J. 1996. Slope instability recognition, analysis, and zonation. *Special Report - National Research Council, Transportation Research Board,* 247**,** 129-177.

THIERY, Y., MALET, J. P., STERLACCHINI, S., PUISSANT, A. & MAQUAIRE, O. 2007. Landslide susceptibility assessment by bivariate methods at large scales: Application to a complex mountainous environment. *Geomorphology,* 92**,** 38-59.

URGELES, R., LEYNAUD, D., LASTRAS, G., CANALS, M. & MIENERT, J. 2006. Back-analysis and failure mechanisms of a large submarine slide on the ebro slope, NW Mediterranean. *Marine Geology,* 226**,** 185-206.

VAN DEN EECKHAUT, M., VANWALLEGHEM, T., POESEN, J., GOVERS, G., VERSTRAETEN, G., & VANDEKERCKHOVE, L. 2006. Prediction of landslide susceptibility using rare events logistic regression: A case-study in the Flemish Ardennes (Belgium). *Geomorphology, 76*(3), 392-410.

VAN WESTEN, C. J., CASTELLANOS, E. & KURIAKOSE, S. L. 2008. Spatial data for landslide susceptibility, hazard, and vulnerability assessment: An overview. *Engineering Geology,* 102**,** 112-131.

VAN WESTEN, C. J., RENGERS, N. & SOETERS, R. 2003. Use of Geomorphological Information in Indirect Landslide Susceptibility Assessment. *Natural Hazards,* 30**,** 399-419.

VAN WESTEN, C. J., RENGERS, N., TERLIEN, M. T. J. & SOETERS, R. 1997. Prediction of the occurrence of slope instability phenomenal through GIS-based hazard zonation. *Geologische Rundschau,* 86**,** 404-414.

VAN WESTEN, C. J., VAN ASCH, T. W. J. & SOETERS, R. 2006. Landslide hazard and risk zonation—why is it still so difficult? *Bulletin of Engineering Geology and the Environment,* 65, 167-184.

CEES J. VAN WESTEN, E. C., SEKHAR L. KURIAKOSE 2008. Spatial data for landslide susceptibility, hazard, and vulnerability assessment: An overview. *Engineering Geology***,** 102, 112 - 131.

VARNES, D. J. 1978. Slope movement types and processes. *Transportation Research Board Special Report,* 176, 11-33.

VORPAHL, P., ELSENBEER, H., MÄRKER, M. & SCHRÖDER, B. 2012. How can statistical models help to determine driving factors of landslides? *Ecological Modelling,* 239**,** 27-39.

YIN, K. L. & YAN, T. Z. 1988. Statistical prediction models for slope instability of metamorphosed rocks *in* Bonnard, C. (Ed.) *Landslides.* Proceeding of the 5th ISL, Lausane. Vol. 2. Balkema, Rotterdam: 1269 - 1272.

ZÊZERE, J., HENRIQUES, C., GARCIA, R., OLIVEIRA, S., PIEDADE, A. & NEVES, M. 2009. Effects of landslide inventories uncertainty on landslide susceptibility modelling. *Mallet, J.-P.; Remaitre, A.; Boggard, T. (Eds.), Landslide Processes: From Geomorphologic Mapping to Dynamic Modelling. CERG Editions, Strasbourg***,** 81-86.

ZÊZERE, J. L., OLIVEIRA, S. C., GARCIA, R. A. C. & REIS, E. 2008. Weighting predisposing factors for shallow slides susceptibility assessment at the regional scale. *Landslides and Engineered Slopes: from the past to the future,* 2, 1831-1837.

Figure Captions

Fig. 1 – Location of the study area. Highlighting the seismic volume BES-100 used in this study.

Fig. 2 – a) Correlation panel between the interpreted seismic units and stratigraphic information from the Espírito Santo Basin based on França et al. (2007). Velocity data for ODP Site 516 was taken from Barker et al. (1993). b) Schematic representation highlighting the study area on the continental slope of Espírito Santo Basin. Figure was modified from e.g. Fiduk et al. (2004); Omosanya and Alves (2013). SR e Syn-Rift sequence, T e Transitional sequence, ED e Early Drift sequence, LD e Late Drift sequence. The area of MTDs area is located in the proximal extensional domain (dashed square).

Fig. 3 - a) Seismic profile highlighting the high amplitude reflector mapped as representing the palaeo topographic surface. The arrows are indicating the horizon mapped to compute the topographic surface; b) 3D view of the topographic surface with a selected inline and crossline, for context. It's the result of the mapped seismic reflector in Fig. 4a and 4c) Seismic profile through the topographic profile of MTD 1. We highlight the reflector of the considered topographic surface which is exactly located beneath the basal reflector of the MTD 1 along its whole MTD.

Fig. 4 - Thematic layers showing the spatial distribution of the predisposing factors considered in the analysis, a) elevation; b) slope gradient; c) profile curvature; d) planform curvature; e) flow direction; d) flow accumulation and g) slope over area ratio

Fig. 5 - Study area offshore Espírito Santo Basin (SE Brazil). The figure shows the location of four MTDs considered in the models. Different shades of grey show the areas of the MTD used for each model. The map shows also the elevation across the study area after depth-converting from time-depth to true-depth.

Fig. 6 - Non-classified MTD predictive maps of offshore Espírito Santo basin (SE Brazil). a) Based on model 1 MTDs group (computed considering the total area of MTDs); b) Based on model 2 (i.e. computed considering 1/3 of total MTDs length) and c) model 3 (computed with half of the area used before). The shape of the MTDs areas in each model are indicated for reference.

Fig. 7 - Cumulative frequency diagram showing the cumulative MTDs occurrence (*y* axis) occurring in the study area classified as susceptible in descending order. Success rate curves of the final models, 1 (AUC= 0.657), 2 (AUC=0.747) and 3 (AUC=0.862).

Fig. 8 - Frequency diagram showing the cumulative area to archive the success-rate curves related to the seven predisposing factors (variables) used into the model 3. The curves are showing how each variable correlate spatially with the MTD.

Fig. 9 – Success rate curves corresponding to MTDs models obtained using from 2 to 7 predisposing factors selected according the sensitivity analysis (2 variables = E+S; 3 variables = E+S+FD; 4 variables = E+S+FD+PlC; 5 variables = E+S+FD+PlC+FA; 6 variables = E+S+FD+PlC+FA+PrC; 7 variables= model 3).

Table 1 - Absolute and relative frequencies for each class of each variable for the seven independent variables (predisposing factors).

Variable	Class Code	Class	N. of pixels	Area of the class (%)
Elevation (m)	E1	0-100	9721	3.2
	E2	100-200	48435	16.0
	E3	200-300	66999	22.0
	E4	300-400	52189	17.2
	E5	400-500	57874	19.2
	E6	500-600	53176	17.4
	E7	600-700	15130	5.0
Slope gradient (º)	S1	[0-1]	108560	35.8
	S2	]1-2]	131386	43.3
	S3	]2-3]	39530	13.0
	S4	]3-4]	12232	4.0
	S5	]4-5]	5377	1.8
	S6	]5-6]	2751	0.9
	S7	]6-7]	1651	0.5
	S8	]7-8]	898	0.3
	S9	>8	1139	0.4
Profile curvature	PrC1	Convex	4151	34.2
	PrC2	Flat	3827	31.5
	PrC3	Concave	4172	34.3
Platform curvature	PlC1	Concave	5556	45.7
	PlC2	Flat	959	7.9
	PlC3	Convex	5635	46.4
Flow	FD1	E	86791	28.6

direction	FD2	SE	86456	28.5
	FD3	S	53672	17.7
	FD4	SW	13530	4.5
	FD5	W	7613	2.5
	FD6	NW	3839	1.3
	FD7	N	14827	4.9
	FD8	NE	36796	12.1
Flow accumulation	FA1	0	67875	22.4
	FA2	1	49210	16.2
	FA3	1-10	126086	41.5
	FA4	10-100	46277	15.2
	FA5	100-1000	12739	4.2
	FA6	>1000	1337	0.4
Slope over area ratio	SAR1	0	9648	3.2
	SAR2	0-0.00001	47399	15.7
	SAR3	0.0000-0.0001	101146	33.6
	SAR4		138112	45.8
	SAR5	0.0001-0.001	4973	1.7
		0.001-0.01		

Table 2 – Morphological characteristics of MTDs interpreted in the Espírito Santo Basin

	Area (km^2)	Volume (km^3)	Max. Thickness (m)	Location
MTD 1	5. 251	0.128	~60	Sub-parallel to slope
MTD 2	20.88	0.659	~65	Upslope to mid-slope
MTD 3	87.180	3.163	~70	Mid-slope to lower slope
MTD 4	19.790	0.470	~80	Sub-parallel to slope

Table 3 - Unstable area in km^2 and relative percentage for the three different models used and total area of the topographic surface for comparison.

	Unstable area (km^2)	**Unstable area (%)**
Model 1	133.8	17.7
Model 2	30.2	4
Model 3	11.1	1.47
Study area	756 km^2	100%

Table 4 – Multicollinearity diagnosis indexes for independent variables used in the models.

Independent variables	**TOL**	**VIF**
- Elevation	0.987	1.013
- Slope gradient	0.866	1.154
- Profile curvature	0.748	1.338
- Planform curvature	0.713	1.402
- Flow direction	0.977	1.024
- Flow accumulation	0.683	1.465
- Slope over area ratio	0.670	1.700

Table 5 - Informative Value scores for each class of each variable for the three models proposed.

		Informative Value		
Variable	**Class Code**	**Model 1**	**Model 2**	**Model 3**
Elevation	E1	-2.527	-3.393	-1.868
	E2	**0.601**	-3.393	-1.868
	E3	**0.286**	-0.542	-1.868
	E4	-0.495	**0.596**	0.858
	E5	-0.118	-0.326	-1.868
	E6	-0.237	**0.877**	**1.171**
	E7	-2.527	-3.393	-1.868
Slope gradient	S1	-0.094	-0.488	-0.586
	S2	**0.128**	0.136	-0.004
	S3	0.002	**0.352**	**0.453**
	S4	-0.273	**0.182**	**0.643**
	S5	-0.337	**0.424**	**0.966**
	S6	-0.401	**0.577**	**1.209**
	S7	-1.208	-0.075	**0.664**
	S8	-1.929	-0.937	-1.191
	S9	-2.007	-0.869	-1.868
Profile curvature	PrC1	0.035	-0.01	0.015
	PrC2	-0.113	-0.231	-0.127
	PrC3	**0.059**	**0.182**	**0.090**
Plan curvature	PlC1	**0.038**	**0.095**	**0.118**
	PlC2	-0.258	-3.393	-0.376

	PlC3	0.0002	-0.044	-0.081
Flow direction	FD1	-0.192	-0.207	-0.381
	FD2	-0.015	**0.168**	**0.120**
	FD3	**0.234**	**0.211**	**0.393**
	FD4	**0.509**	-0.688	-0.562
	FD5	**0.237**	-0.731	-0.358
	FD6	**0.067**	-0.209	**0.352**
	FD7	-0.141	-0.117	**0.183**
	FD8	-0.219	**0.024**	-0.174
Flow accumulation	FA1	0.008	-0.130	-0.132
	FA2	0.004	-0.080	-0.065
	FA3	0.001	0.060	**0.088**
	FA4	-0.009	-0.004	-0.023
	FA5	-0.080	**0.129**	-0.117
	FA6	**0.342**	**1.094**	**1.014**
Slope over area ratio	SAR1	**0.196**	-0.175	**0.430**
	SAR2	-0.052	**0.049**	-0.103
	SAR3	0.001	**0.016**	-0.085
	SAR4	0.018	-0.003	0.065
	SAR5	-0.596	-0.324	-0.364

Table 6 - Hierarchy of predisposing factors for MTDs occurrences, according to success rate curves and AUC (Area Under the Curve), regarding model 3.

Ranking	Variable	AUC
1	Elevation	0.832
2	Slope gradient	0.616
3	Flow direction	0.584
4	Plan curvature	0.542
5	Flow accumulation	0.537
6	Profile curvature	0.534
7	Slope over area ratio	0.493

Table 7 - Area under the curve (AUC) of success rate curves corresponding to the model 3 obtained using from 2 to 7 predisposing factors

Variable	AUC
2 variables (Variable Id: E+S)	0.8543
3 variables (Variable Id: E+S+FD)	0.8603
4 variables (Variable Id: E+S+FD+PlC)	0.8619
5 variables (Variable Id: E+S+FD+PlC+FA)	0.8619
6 variables (Variable Id: E+S+FD+PlC+FA+PrC)	0.8616
7 variables (Variable Id: E+S+FD+PlC+FA+PrC+SAR)	0.8615

Highligts

- The use of 3D seismic dataset as source of information to GIS modelling;
- GIS statistical modelling to the submarine slope instabilities
- Understanding terrain conditions for submarine slope stability analyses;
- Statistical/probabilistic analysis to understand the conditions and parameters that favour the occurrence of MTDs in a specific location.

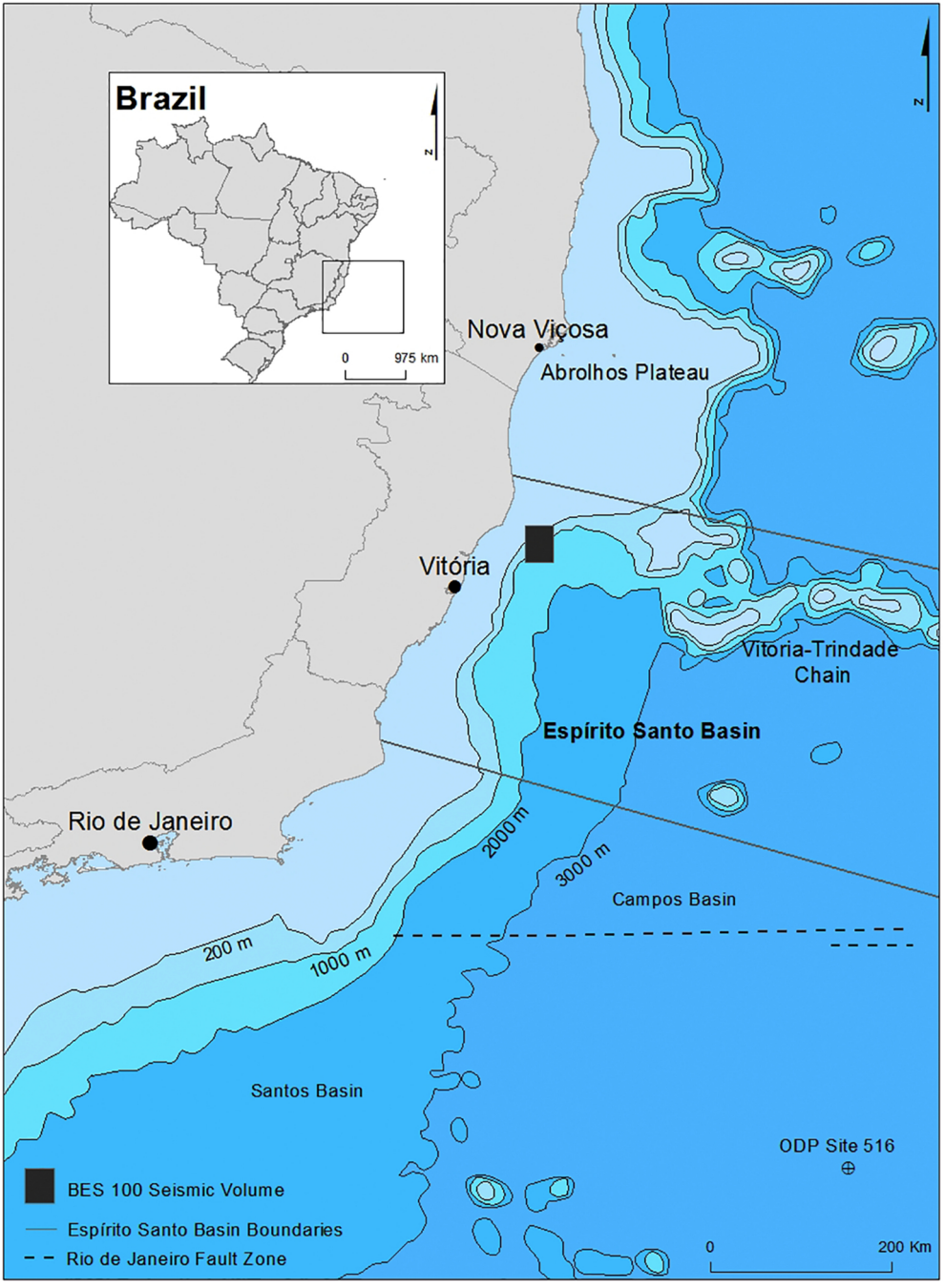
Brazil
N
0
975 km
Nova Viçosa
Abrolhos Plateau
Vitória
Vitoria-Trindade
Chain
Espírito Santo Basin
Rio de Janeiro
2000 m
3000 m
Campos Basin
200 m
1000 m
Santos Basin
ODP Site 516
BES 100 Seismic Volume
Espírito Santo Basin Boundaries
Rio de Janeiro Fault Zone
0
200 Km

Figure 1

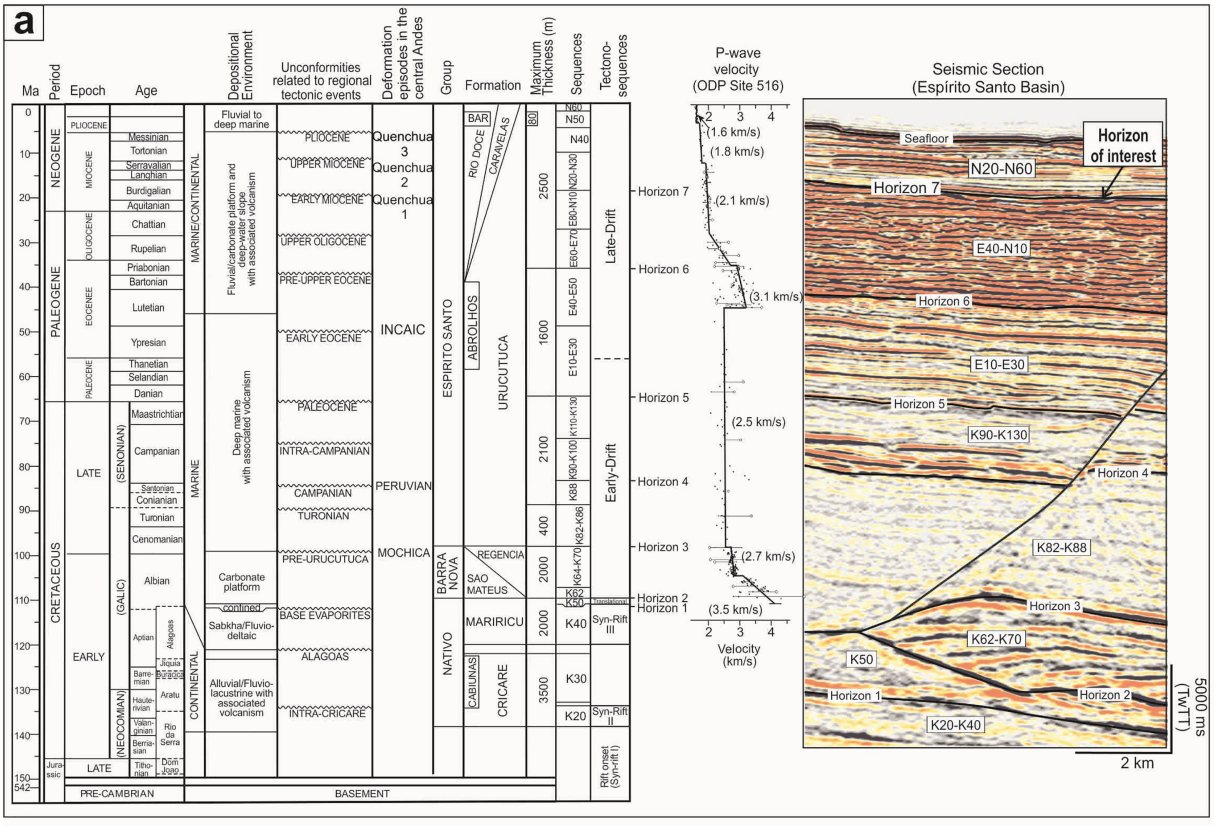
a
Ma
Period
Epoch
Age
Depositional Environment
Unconformities related to regional tectonic events
Deformation episodes in the central Andes
Group
Formation
Maximum Thickness (m)
Sequences
Tectono-sequences
P-wave velocity (ODP Site 516)
Seismic Section (Espírito Santo Basin)
Horizon of interest
Seafloor
Horizon 7
Horizon 6
Horizon 5
Horizon 4
Horizon 3
Horizon 2
Horizon 1
N20-N60
E40-N10
E10-E30
K90-K130
K82-K88
K62-K70
K50
K20-K40
(1.6 km/s)
(1.8 km/s)
(2.1 km/s)
(3.1 km/s)
(2.5 km/s)
(2.7 km/s)
(3.5 km/s)
Velocity (km/s)
5000 ms (TWTT)
2 km
NEOGENE
PALEOGENE
CRETACEOUS
MARINE/CONTINENTAL
MARINE
CONTINENTAL
ESPIRITO SANTO
ABROLHOS
URUCUTUCA
BARRA NOVA
NATIVO
REGENCIA
SAO MATEUS
MARIRICU
CABIUNAS
CRICARE
BAR
RIO DOCE
CARAVELAS
Late-Drift
Early-Drift
Syn-Rift III
Syn-Rift II
Rift onset (Syn-rift I)
PRE-CAMBRIAN
BASEMENT

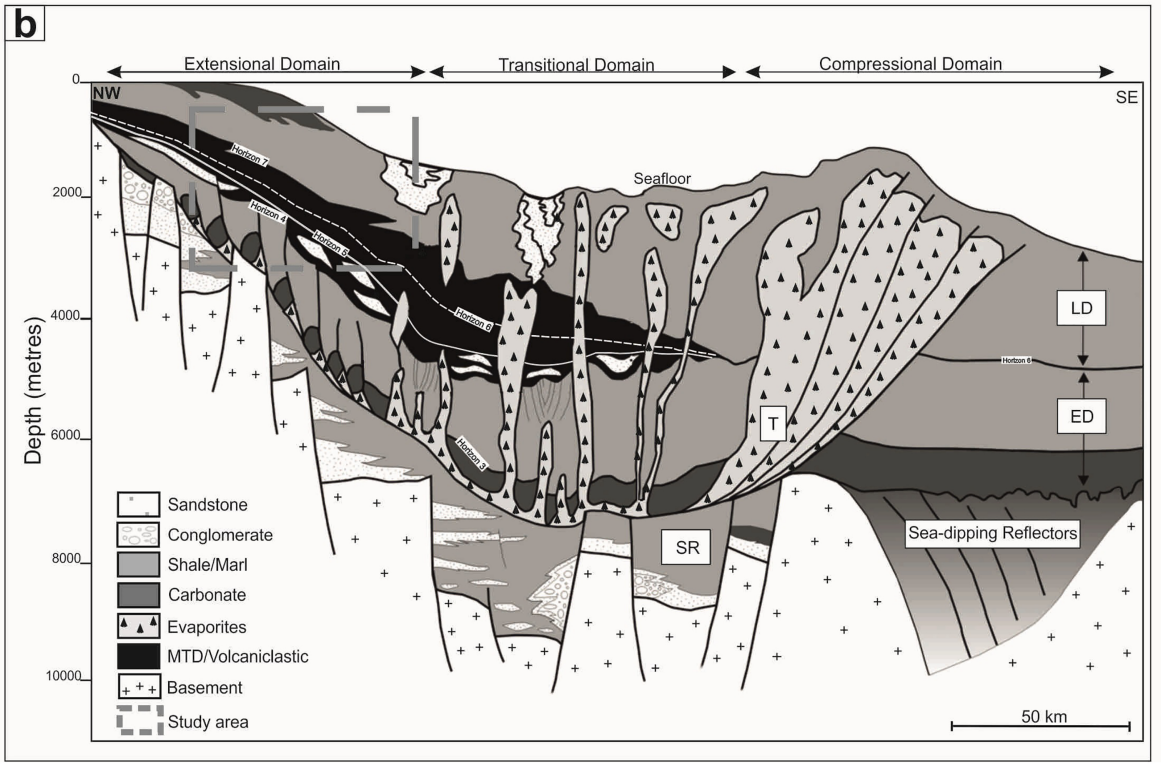
b
Extensional Domain
Transitional Domain
Compressional Domain
NW
SE
Seafloor
Horizon 7
Horizon 4
Horizon 6
Horizon 8
Horizon 5
LD
ED
T
SR
Sea-dipping Reflectors
Depth (metres)
Sandstone
Conglomerate
Shale/Marl
Carbonate
Evaporites
MTD/Volcaniclastic
Basement
Study area
50 km

Figure 2

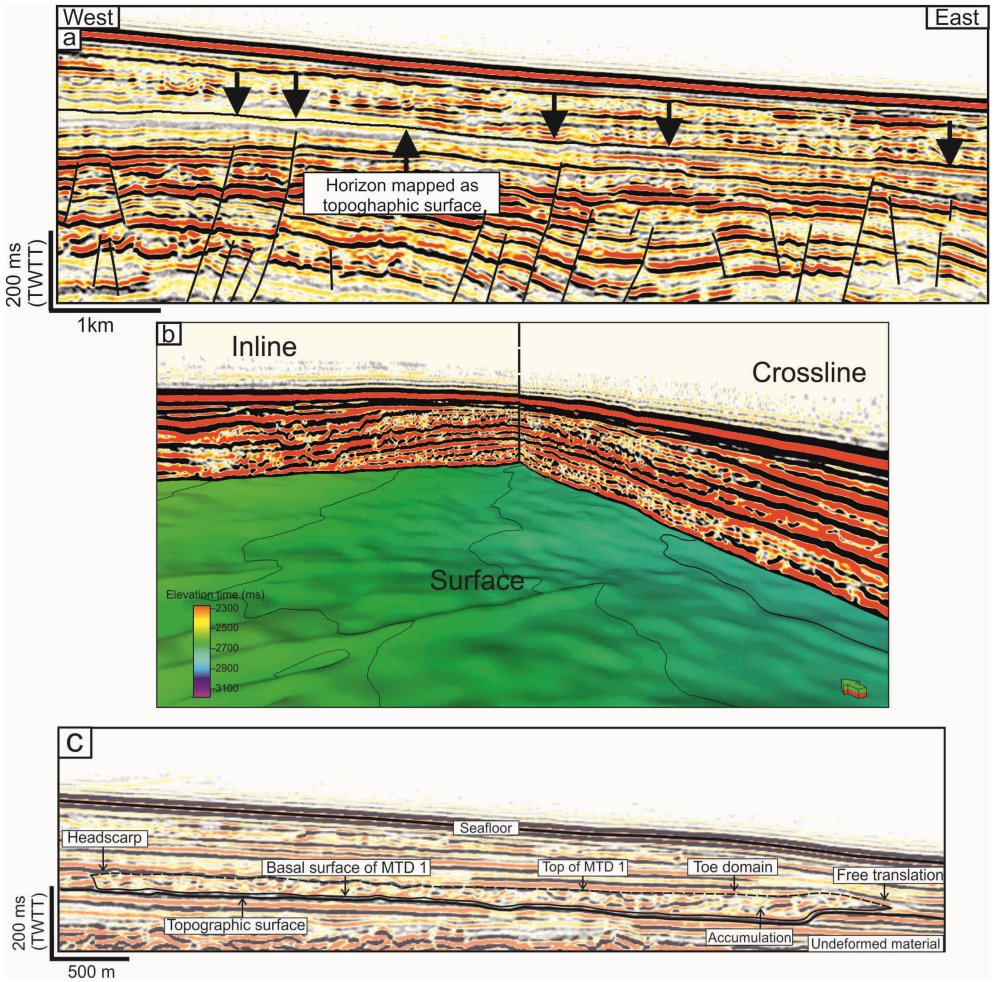
West
East
a
Horizon mapped as topoghaphic surface
200 ms (TWTT)
1km
b
Inline
Crossline
Surface
Elevation time (ms)
2300
2500
2700
2900
3100
c
Headscarp
Seafloor
Basal surface of MTD 1
Top of MTD 1
Toe domain
Free translation
Topographic surface
Accumulation
Undeformed material
200 ms (TWTT)
500 m

Figure 3

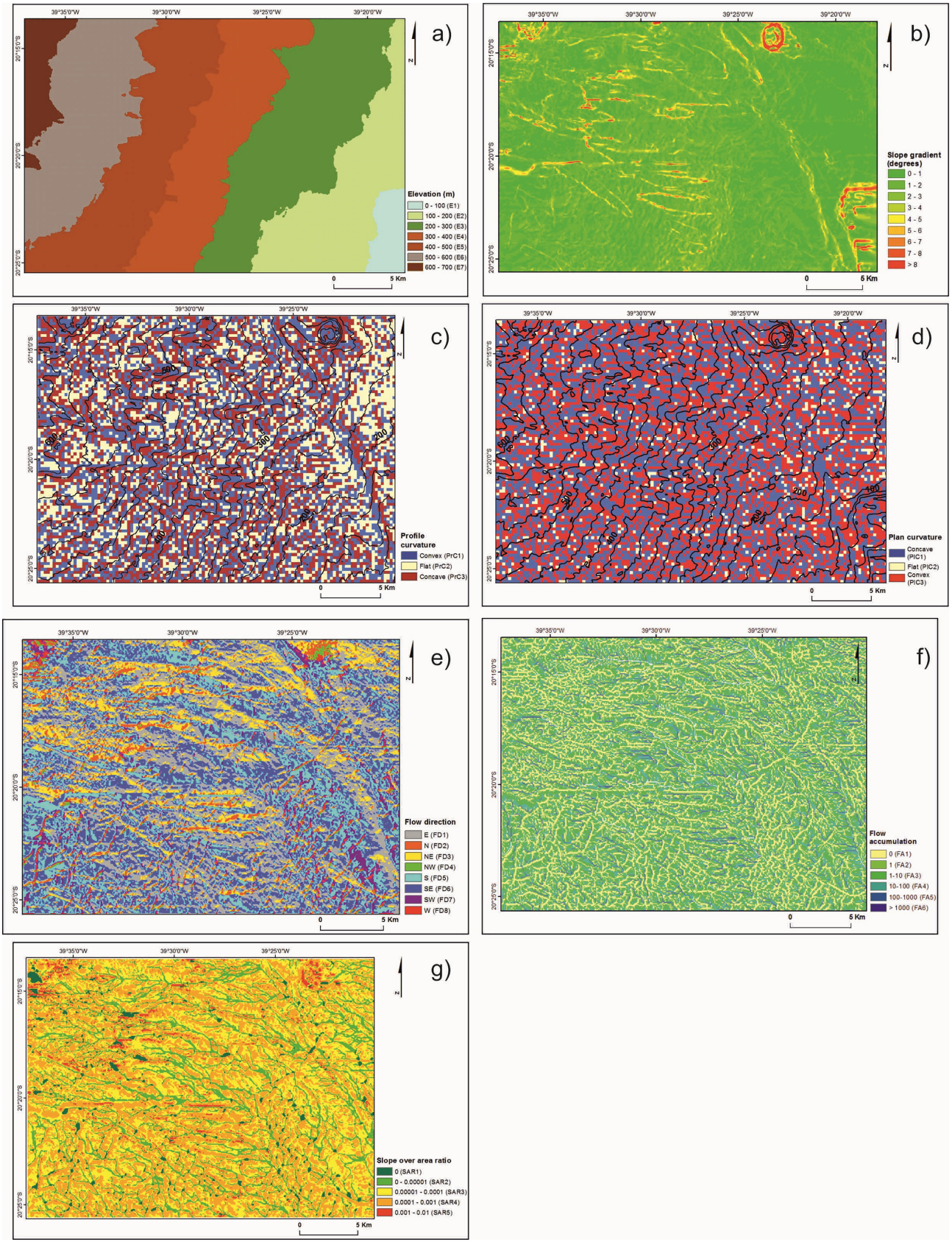
a)
39°35'0"W
39°30'0"W
39°25'0"W
39°20'0"W
20°15'0"S
20°20'0"S
20°25'0"S
N
Elevation (m)
0 - 100 (E1)
100 - 200 (E2)
200 - 300 (E3)
300 - 400 (E4)
400 - 500 (E5)
500 - 600 (E6)
600 - 700 (E7)
0
5 Km
b)
Slope gradient (degrees)
0 - 1
1 - 2
2 - 3
3 - 4
4 - 5
5 - 6
6 - 7
7 - 8
> 8
c)
Profile curvature
Convex (PrC1)
Flat (PrC2)
Concave (PrC3)
d)
Plan curvature
Concave (PlC1)
Flat (PlC2)
Convex (PlC3)
e)
Flow direction
E (FD1)
N (FD2)
NE (FD3)
NW (FD4)
S (FD5)
SE (FD6)
SW (FD7)
W (FD8)
f)
Flow accumulation
0 (FA1)
1 (FA2)
1-10 (FA3)
10-100 (FA4)
100-1000 (FA5)
> 1000 (FA6)
g)
Slope over area ratio
0 (SAR1)
0 - 0.00001 (SAR2)
0.00001 - 0.0001 (SAR3)
0.0001 - 0.001 (SAR4)
0.001 - 0.01 (SAR5)

Figure 4

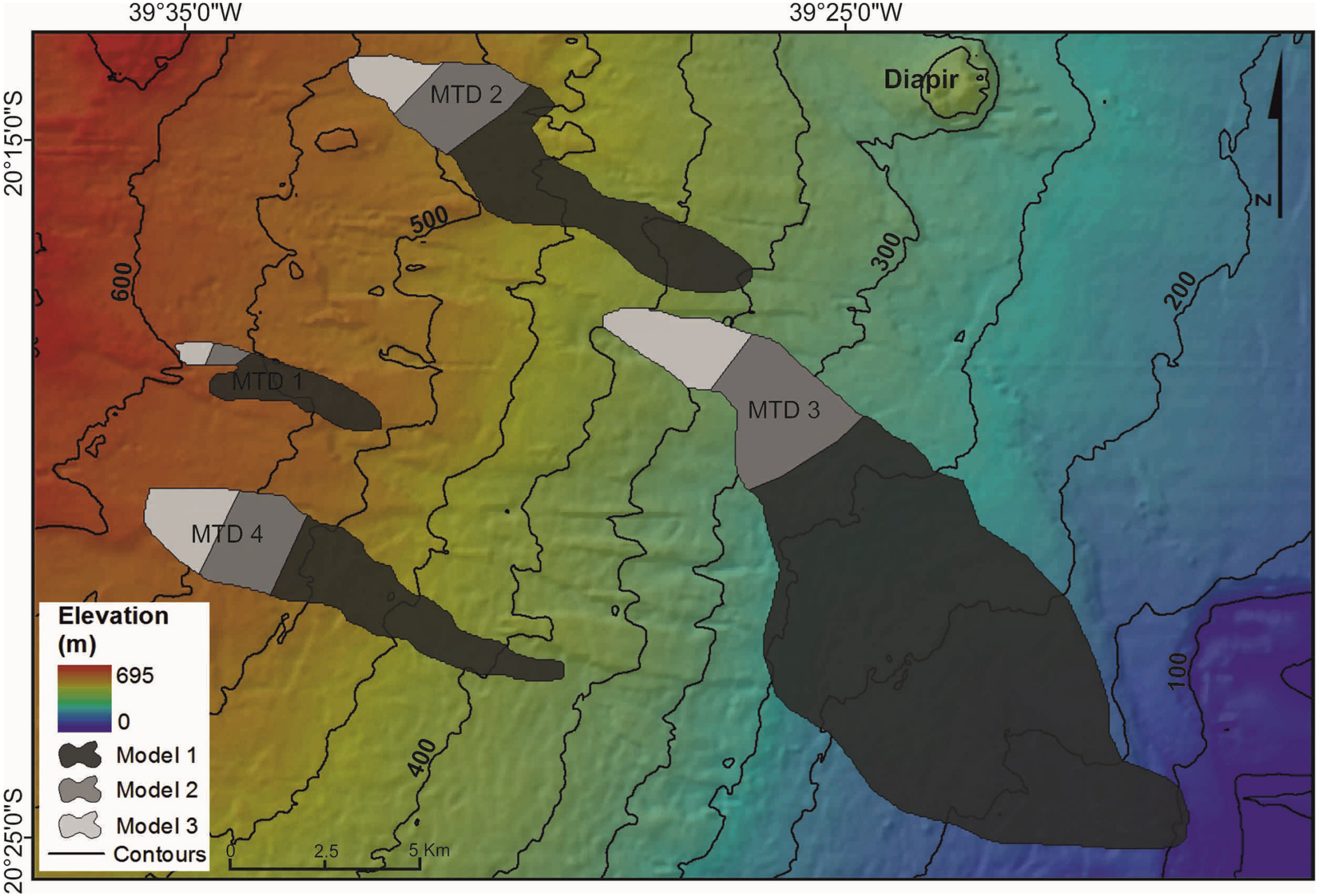
39°35'0"W
39°25'0"W
20°15'0"S
20°25'0"S
MTD 1
MTD 2
MTD 3
MTD 4
Diapir
600
500
400
300
200
100
N
Elevation (m)
695
0
Model 1
Model 2
Model 3
Contours
0
2.5
5 Km

Figure 5

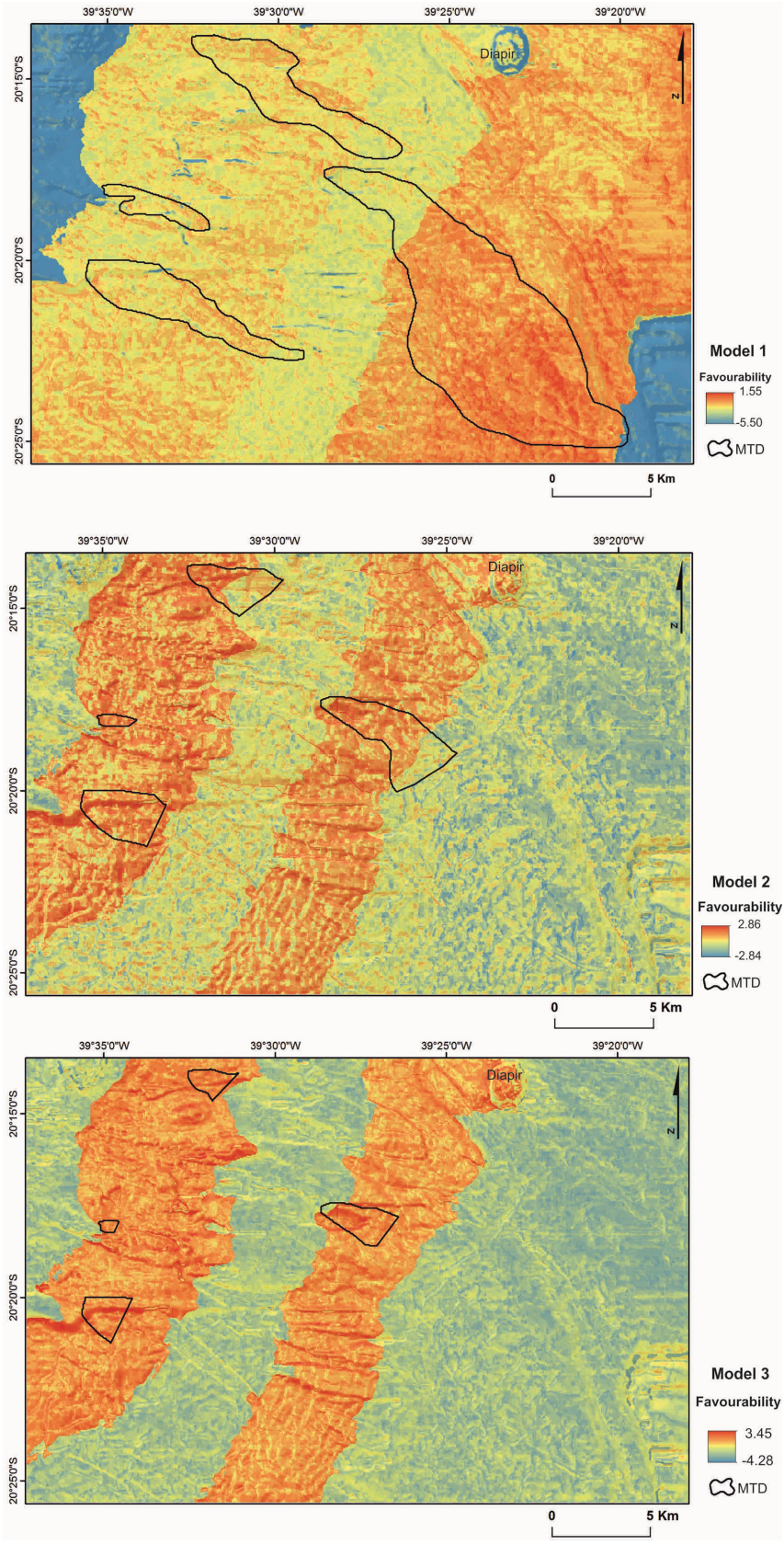
39°35'0"W
39°30'0"W
39°25'0"W
39°20'0"W
20°15'0"S
20°20'0"S
20°25'0"S
Diapir
N
Model 1
Favourability
1.55
-5.50
MTD
0
5 Km
Model 2
Favourability
2.86
-2.84
MTD
Model 3
Favourability
3.45
-4.28
MTD

Figure 6

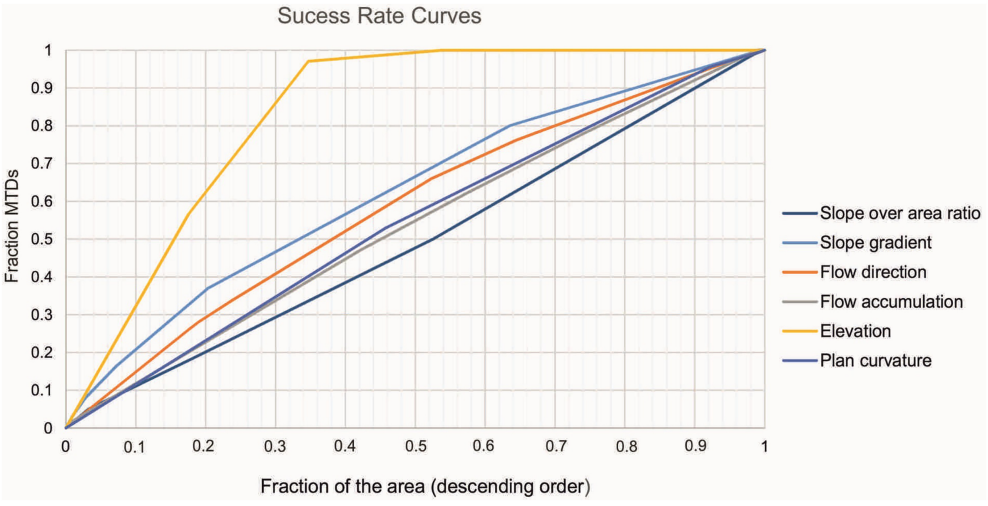
Sucess Rate Curves
Fraction MTDs
Fraction of the area (descending order)
0
0.1
0.2
0.3
0.4
0.5
0.6
0.7
0.8
0.9
1
Slope over area ratio
Slope gradient
Flow direction
Flow accumulation
Elevation
Plan curvature

Figure 7

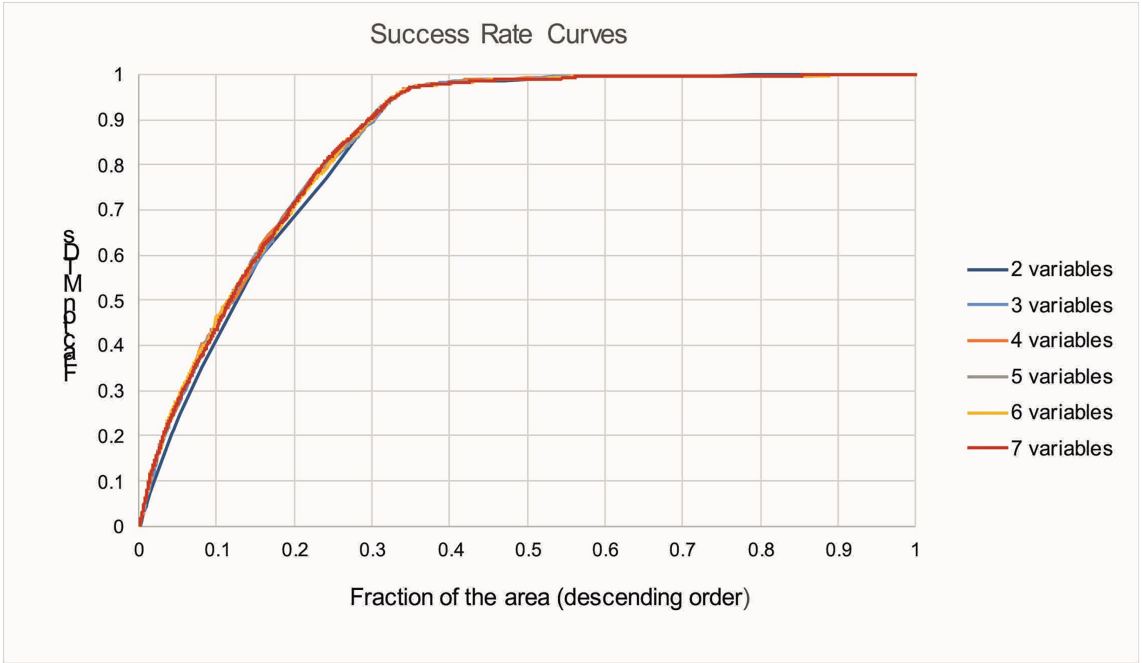
Success Rate Curves
1
0.9
0.8
0.7
0.6
0.5
0.4
0.3
0.2
0.1
0
0
0.1
0.2
0.3
0.4
0.5
0.6
0.7
0.8
0.9
1
Fraction of the area (descending order)
2 variables
3 variables
4 variables
5 variables
6 variables
7 variables

Figure 8

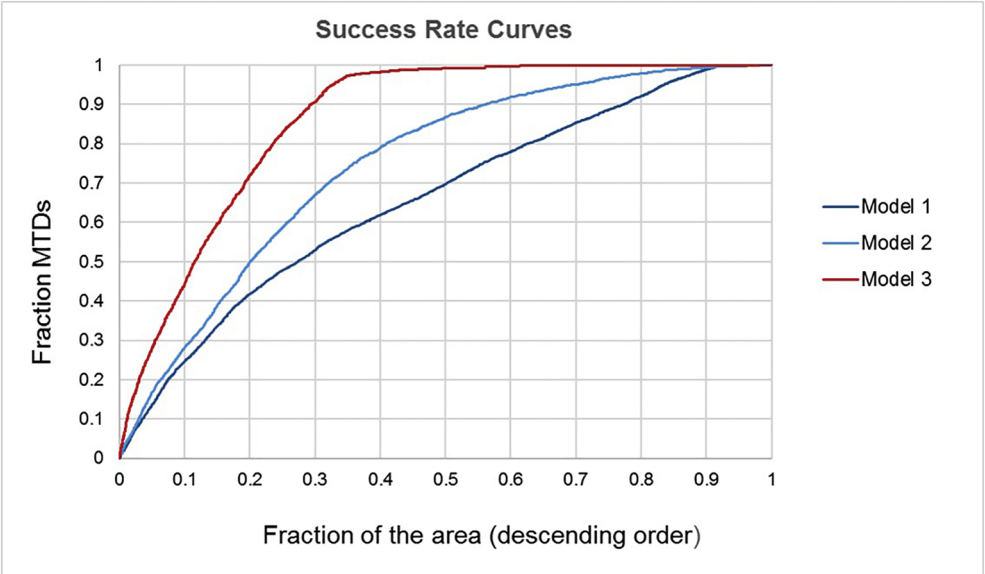
Success Rate Curves
Fraction MTDs
1
0.9
0.8
0.7
0.6
0.5
0.4
0.3
0.2
0.1
0
0
0.1
0.2
0.3
0.4
0.5
0.6
0.7
0.8
0.9
1
Fraction of the area (descending order)
Model 1
Model 2
Model 3

Figure 9